Spectrochimica Acta Part B 64 (2009) 126–140

Contents lists available at ScienceDirect

Spectrochimica Acta Part B

journal homepage: www.elsevier.com/locate/sab

Hybrid Monte Carlo — Fluid model for studying the effects of nitrogen addition to argon glow discharges

Annemie Bogaerts

University of Antwerp, Department of Chemistry, Research group PLASMANT, Universiteitsplein 1, B-2610 Wilrijk-Antwerp, Belgium

ARTICLE INFO

Article history:
Received 9 September 2008
Accepted 19 November 2008
Available online 28 November 2008

Keywords:
Glow discharge
Grimm-source
Computer simulation
Modeling
Argon/nitrogen
Gas mixture
Nitrogen addition

ABSTRACT

A computer model is developed for describing argon/nitrogen glow discharges. The species taken into account in the model include electrons, Ar atoms in the ground state and in the 4s metastable levels, N_2 molecules in the ground state and in six different electronically excited levels, N atoms, Ar^+ ions, N^+, N_2^+, N_3^+ and N_4^+ ions. The fast electrons are simulated with a Monte Carlo model, whereas all other species are treated in a fluid model. 74 different chemical reactions are considered in the model. The calculation results include the densities of all the different plasma species, as well as information on their production and loss processes. The effect of different N_2 additions, in the range between 0.1 and 10%, is investigated.

1. Introduction

It is well known that the working conditions in glow discharges may be considerably affected by small amounts of molecular gases, such as nitrogen, in the discharge gas (e.g., [1–14]). In glow discharge optical emission spectrometry (GD-OES), the intensities of emission lines can change drastically, thereby influencing significantly the quantitative analysis. This is a critical observation, because in many samples, these gaseous elements are present as compounds or occluded gas. Furthermore, traces of nitrogen are omnipresent in the discharge, due to minor vacuum leaks in the glow discharge source.

Bengtson [1] reported that substantial molecular emission and interferences, identified as originating from diatomic species, such as CH, OH, NH and CO, were observed in the spectrum of organic coatings. The observed molecular bands overlap with several atomic emission lines, causing line interferences. The impact of molecular emission on compositional depth profiling with GD-OES was further discussed in a recent viewpoint article by Bengtson [2]. An important observation was that dissociation and subsequent recombination processes occur, leading to the formation of molecular species, which were not present in the original plasma gas. A literature overview of observations of molecular emission in glow discharge plasmas was also given and characteristics of molecular emission spectra were briefly discussed. With respect to N_2 addition, very strong emission from several bands of N_2 was demonstrated, mostly from the Second Positive C $^3\Pi_u$–B $^3\Pi_g$ system, and this can interfere with a large number of analytical atomic lines, showing that even minor vacuum leaks can lead to artifacts in the form of false elemental signals [2].

For this reason, several experiments have been conducted already by various research groups, for studying the effects of small N_2 concentrations in the discharge. In [3] the effects of a controlled addition of N_2 and O_2 on the analytical parameters, such as the effective sputtering rate, the emission intensity of several spectral lines and the electrical current in GD-OES, was investigated. The general effect of the gaseous addition was a decrease in the sputtering rate [3]. Wagatsuma gave an overview of emission characteristics of mixed gas plasmas, such as Ar–N_2 [4]. It is illustrated that the use of mixed plasma gases does not always exert a positive influence on the analytical performance of GD-OES, although it can be a possible option to improve the analytical performance.

Smid et al. carried out a very interesting and detailed study on the effect of N_2 on analytical glow discharges by high resolution Fourier Transform UV–VIS spectrometry [5]. Intensities and line profiles of emission lines originating from argon, the sample and nitrogen (atomic and molecular bands) were recorded over a wide spectral region. Among other results, it was shown that the self-reversal for the ArI 811.5 nm and ArI 763.5 nm resonance lines was reduced upon N_2 addition, which suggests a reduction in the Ar metastable atom population [5].

Fernandez et al. [6,7] investigated the effect of adding either H_2, N_2 or O_2 (from 0.5 to 10% v/v) to an Ar rf glow discharge. A decrease in the sputtering rates was observed in the three cases, as well as selective enhancements in the emission yields for some lines, upon addition of H_2 or N_2 [6]. An enhancement in the dc bias was observed for N_2 concentrations in the interval 2–10% v/v. Furthermore, the crater shapes appeared to be modified upon addition of these gases, yielding

E-mail address: Annemie.bogaerts@ua.ac.be.

0584-8547/$ – see front matter © 2008 Elsevier B.V. All rights reserved.
doi:10.1016/j.sab.2008.11.004

more convex or concave craters, at high or low power, respectively. It was concluded that plasma gas mixtures can offer a great potential to improve depth resolution in rf GD-OES [7]. The same research group [8] studied the effect of N_2 on the calibration curves of various emission lines in GD-OES. Negligible differences were observed in the calculated emission yields for samples with and without nitrogen in their composition. However, when Ar/N_2 mixtures (with 0.5% v/v N_2 concentration) were investigated, differences in the slopes of the calibration curves up to 30% were detected. Also the molecular bands recorded in the spectra when N_2 is present were investigated and the resulting interferences on the analytes were determined.

Some other effects of N_2 addition on the discharge characteristics have also been observed. For instance in [9] it was reported that very small amounts of a molecular additive, such as N_2, can drastically alter the behavior of the electron drift velocity, and Kimura et al. [10] demonstrated that the electron energy distribution function in the positive column of Ar/N_2 glow discharges was greatly affected by the amount of N_2. Steers et al. [11] showed that the volt–ampere characteristics were different in Ar–N_2 mixtures compared to pure Ar discharges. More specifically, the discharge resistance increases, hence yielding a lower electrical current at constant voltage and pressure, or a higher voltage at constant pressure and current [11].

In order to obtain a better insight in the underlying mechanisms responsible for the effects of N_2 addition to an Ar plasma, computer modeling can be very useful. In the literature, some models have already been reported, describing N_2 and Ar/N_2 discharges, because these kinds of plasmas are widely used for plasma processing applications, such as for the deposition of Fe_4N coatings or steel nitriding [12]. Furthermore, Ar/N_2 discharges are nowadays gaining increasing interest in the magnetron reactive sputter deposition process of all kinds of nitride films [13].

Loureiro and Fereira [14,15] have developed a model for N_2 stationary and high-frequency discharges, based on balance equations for the N_2 molecules in various vibrationally excited levels, and the Boltzmann equation for the electron behavior [16]. A similar model was reported for a N_2/H_2 glow discharge by Loureiro and Ricard [17] and by Capitelli et al. [18]. Guerra and Loureiro have extended the model developed in [14,15] to a N_2/O_2 stationary discharge [19], including also NO, N (^{4}S) and O (^{3}P) species, besides the N_2 and O_2 molecules in various vibrationally excited levels. This model was further extended by the same authors in [20] to include balance equations for the N_2 molecules in various electronically excited levels, as well as N_2^+, N_4^+, O^+, O_2^+ and NO^+ ions. Kossyi et al. have also developed a model for a non-equilibrium discharge in a N_2/O_2 mixture [21]. In [22] the basic bulk and surface processes in dc and microwave discharge plasmas in N_2, O_2, H_2 and their mixtures were reviewed, and a comparison between model predictions and experiments was presented.

In [23] Guerra and Loureiro further improved their model by including also various N_2 electronically excited molecules, and applied it to the positive column of a pure N_2 low pressure glow discharge. Sa and Loureiro extended this model to the afterglow of a microwave plasma, in pure N_2 as well as in a N_2/Ar mixture, with fractional Ar concentrations varying between 0 and 90% [24]. Petrov et al. developed a similar model for an atmospheric pressure capillary surface wave discharge in a He/N_2 mixture [25]. The influence of small N_2 concentrations (typically less than 1%) on the discharge characteristics was studied and compared with experimental data. It was found that under such conditions N_2 is highly dissociated (up to 70% at very low N_2 additions) and that the density of metastable He atoms is greatly reduced upon N_2 addition, even at such low concentrations of 0.03%.

Tatarova and colleagues presented a model for surface wave sustained discharges in pure N_2 [26] and extended the model later to a wave-driven N_2–Ar discharge, with Ar concentration varying between 10 and 95% [27]. This model was validated by a companion experimental paper [28]. In another paper, wave-driven H_2, N_2 and N_2–Ar discharges were modeled [29]. It was stated that N_2^+ ions were the dominant ions over a wide range of Ar–N_2 mixing ratios, due to the fast charge transfer between Ar^+ ions and N_2 molecules and associative ionization from N_2 (A) metastable molecules. Furthermore, the dissociation degree appeared to increase upon addition of Ar, as a result of the above charge transfer process, followed by dissociative recombination of N_2^+ ions [27–29].

Debal et al. have developed a collisional-radiative model for an Ar/N_2 magnetron discharge, including several electronically excited N_2 molecules, several excited levels of the N atoms, as well as the N^+ and N_2^+ ions [30]. The modeling results have been compared with optical emission spectrometry. The emission intensity variations of plasma species have been analyzed vs. the nitrogen relative concentration and the electrical power, and compared with calculated populations of the emitting species. Reasonable agreement between calculation results and experiments was obtained. A typical dissociation degree of 0.13–0.24% was predicted, depending on the fractional N_2 concentration. The ionization degree of N_2 was even a bit lower, with N_2^+ being the major nitrogen ionic species [30]. Kimura et al. [10] presented also a model, based on the Boltzmann equation and the rate equations for electrons and excited particles in an Ar/N_2 positive column glow discharge. A comparison was made between measured and calculated electron energy distribution functions, and qualitative agreement was reached.

In the present paper, we describe a computer model specifically designed for analytical Ar/N_2 glow discharges, although it is of course also applicable to other glow discharges, operating at similar conditions. This model is largely based on the models reported in [23–25,27]. However, in first instance, we have neglected the vibrational kinetics of the N_2 molecules, and we consider only electronically excited N_2 molecules. Indeed, it is reported [25] that these vibrational kinetics are especially important for the electron energy distribution function in the low energy range, as vibrational excitation is characterized by low threshold energies. However, our model is applied to glow discharges operating at high voltages (order of 1 kV), where the electrons can have rather high energies, and moreover, we are especially interested in the electronically excited levels (for the application of GD-OES) and the behavior of the various ions (for glow discharge mass spectrometry; GDMS), and it is reported that the vibrational kinetics are of lower importance for these species [25]. Moreover, the N_2 dissociation due to vibration–vibration (V–V) and vibration–translation (V–T) energy exchanges is shown to represent only a minor contribution to the total rate of dissociation [23].

2. Description of the model

The different plasma species considered in our model are presented in Table 1. Besides the Ar atoms (in the ground state and excited to the metastable ($3p^5\ 4s\ ^3P_2$) level at 11.55 eV), the Ar^+ ions and electrons, several nitrogen species are also included, i.e., four types of ions, the ground state N atoms, as well as N_2 molecules in the ground state and in various electronically excited levels. In the table, both the full notation and the short notation, as will be used further in this paper,

Table 1
Different plasma species included in the model

Ground state neutrals	Neutrals in excited state	Ions	Electrons
Ar^0	Ar_m* (in metastable level)	Ar^+	e^-
N_2 (X) (X $^1\Sigma_g^+$)	N_2 (A) (A $^3\Sigma_u^+$)	N_2^+, N_3^+, N_4^+	
	N_2 (B) (B $^3\Pi_g$)		
	N_2 (a′) (a′ $^1\Sigma_u^-$)		
	N_2 (a) (a $^1\Pi_g$)		
	N_2 (w) (w $^1\Delta_u$)		
	N_2 (C) (C $^3\Pi_u$)		
N (^{4}S)		N^+	

For the N_2 molecules in ground and excited levels, both the short notation (as used further in this paper) and the full notation are given.

are presented for these molecular levels. A schematic diagram of these excited levels (i.e., their potential energy curves as a function of interatomic distance) is illustrated in Fig. 1. It should be noted that the N_2 (B' $^3\Sigma_u^-$) level is not explicitly included in the model, but it is indirectly taken into account, as it is assumed to be only populated by electron impact excitation from the N_2 ground state and rapidly depopulated by radiative decay to the N_2 (B $^3\Pi_g$) level. Hence, in our model the electron impact excitation rate to this N_2 (B' $^3\Sigma_u^-$) level is therefore directly used as production rate for the N_2 (B $^3\Pi_g$) level. Also the N_2 (a'' $^1\Sigma_g^+$) level is neglected in our model, because it is rapidly quenched upon collisions with electrons, at a rate constant of 2.3×10^{-10} cm^3 s^{-1} [31]. For the N atoms, only the ground state (^{4}S) is included, because the excited levels have much lower densities. Indeed, it is demonstrated [23] that the conversion of N(^{4}S) to the atomic metastable state N(^{2}P) upon collisions with N_2(A) molecules is not an effective depopulating mechanism for the N(^{4}S) atoms, as most of the N(^{2}P) atoms created in this way will be rapidly reconverted to the N(^{4}S) atoms by collisions on the walls and quenching [23]. It should be mentioned, however, that this process is still taken into account in the model as a loss mechanism for the N_2(A) molecules (see below).

All these species are treated either with a Monte Carlo or a fluid model. More specifically, the electrons are split up in two groups; the so-called fast electrons, with energies above the threshold for inelastic collisions, are described with a Monte Carlo approach, whereas the so-called thermal electrons are handled with a fluid model. All the other plasma species are also treated with a fluid model (see below).

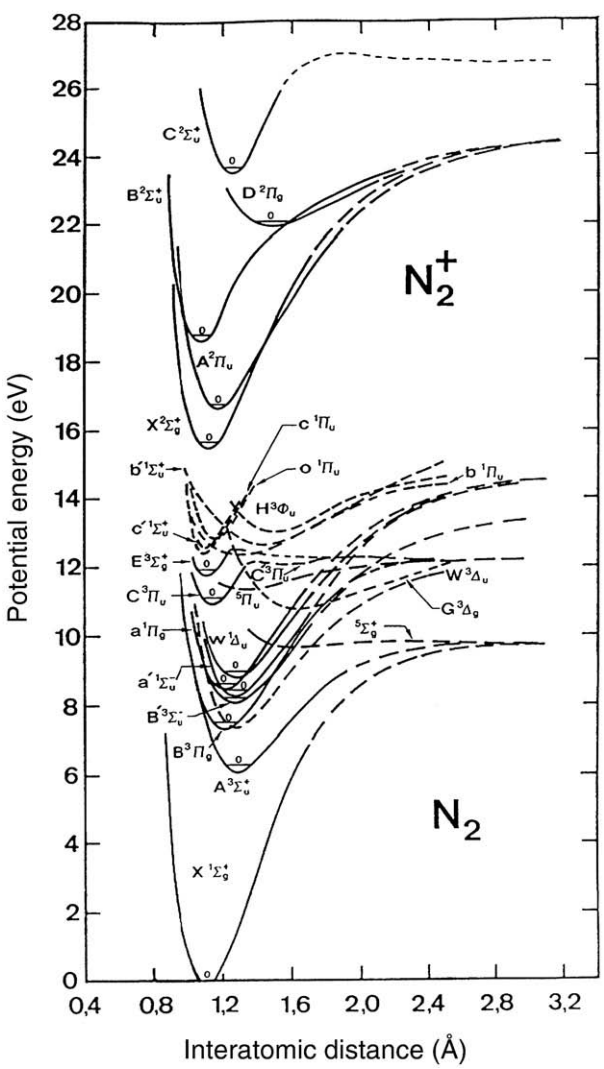

Fig. 1. Schematic diagram of the potential energy curves of N_2 molecules (and N_2^+ ions). The N_2 energy levels included in our model, are summarized in Table 1.

The various chemical reactions of the plasma species are listed in Tables 2–4. Table 2 contains the electron reactions. Most of these reactions are described in the electron Monte Carlo model, based on the energy-dependent cross sections, which are illustrated in Fig. 2. The labels on the curves in this figure correspond to the numbers in Table 2. The electron-ion recombination processes, listed as numbers 19–26 in Table 2, are however treated in the fluid model, as they are occurring for the thermal electrons. The rates of these processes are calculated based on rate coefficients, which are included in Table 2.

Table 3 illustrates the reactions of the various ions, which are also treated in the fluid model. The corresponding rate coefficients are also given in the table. For most reactions, rate coefficients could be found, but for the asymmetric charge transfer reactions, some assumptions had to be made. Indeed, in [42] rate coefficients for the asymmetric charge transfer reaction between Ar^+ and N_2 were reported, as a function of vibrational temperature and vibrational energy level. The rate coefficient increases from a value of 1.2×10^{-11} cm^3 s^{-1} at a N_2 vibrational temperature of 300 K to a value of 2×10^{-11} cm^3 s^{-1} for a N_2 vibrational temperature of 4700 K. Based on these data, rate coefficients were derived for specific vibrational levels, and values were obtained of 1.2×10^{-11} cm^3 s^{-1} for $v=0$, 3×10^{-10} cm^3 s^{-1} for $v=1$, 7.6×10^{-10} cm^3 s^{-1} for $v=2$ and 3, and lower values for higher vibrational levels [42]. Similarly, for the asymmetric charge transfer reaction between N_2^+ and Ar, the rate coefficients were also found to be different depending on the N_2^+ vibrational level, ranging between 10^{-11} cm^3 s^{-1} for $v=0$, and about 4×10^{-10} cm^3 s^{-1} for $v=1$–4 [43]. Since we have not taken into account the vibrational kinetics of the N_2 molecules and N_2^+ ions, it is difficult to deduce which value is most realistic for our conditions. We have therefore adopted the values used in [27], because these calculation results were validated by experiments [28]. However, it should be realized that the model of [27] applies to another type of discharge, so it is not sure that the N_2 and N_2^+ species are in the same vibrational levels. Therefore, we have also performed a series of calculations, varying these rate coefficients in the range reported in [42,43], to investigate the sensitivity of the calculation results on these rate coefficients.

For the other charge transfer reactions listed in Table 3, also some assumptions had to be made, but they were less critical, because these reactions are of lower importance, due to the lower number densities of the reacting species. For the asymmetric charge transfer of Ar^+ with N atoms (reaction 28), the same value was assumed as for reaction 27, and the same applies for reaction 29, as these are reactions with good energy overlap (or exothermic reactions). Reaction 30, on the other hand, is an endothermic reaction, which will be characterized by a lower rate constant. We estimated it, from the rate coefficient for the reverse reaction (i.e., reaction 28), based on the energy difference between the levels: $k_{30}=k_{28}\exp(-\Delta E/kT)$. For an energy difference of 0.23 eV and a gas temperature of 300 K, this yields a value of 6×10^{-14} cm^3 s^{-1}. Finally, the rate coefficients for reactions (39) and (40) were assumed to be the same as for reaction (38), and the one for reaction (43) was taken the same as for reaction (42).

The reactions involving the neutral species (i.e., nitrogen molecules and atoms, as well as Ar metastable atoms), are listed in Table 4, as well as their corresponding rate coefficients. Besides chemical reactions, also some radiative decay processes are included in the model for the electronically excited N_2 levels, and the corresponding Einstein transition probabilities are also listed in Table 4.

As mentioned above, these chemical reactions are defined as production and loss rates for the various species in a fluid model. Indeed, for every species, a continuity equation (balance equation) is constructed, based on production and loss rates. Furthermore, a flux equation, based on diffusion for the neutral species, and on diffusion and migration for the ions and electrons, determines the transport of all the species. The diffusion coefficients were calculated with a formula of the

Table 2
Overview of the electron reactions taken into account in the model, as well as the corresponding rate coefficients (or cross sections) and the references where these data are adopted from

No.	Reaction	Name	k (or σ)	Ref.
1	$e^- + Ar \rightarrow e^- + Ar$	Elastic collisions with Ar	$\sigma(E)$	[32]
2	$e^- + Ar \rightarrow 2\ e^- + Ar^+$	Ionization of Ar	$\sigma(E)$	[32]
3	$e^- + Ar \rightarrow e^- + Ar^*$ (total)	Total excitation of Ar	$\sigma(E)$	[32]
4	$e^- + Ar \rightarrow e^- + Ar_m^*$	Excitation to Ar_m^*	$\sigma(E)$	[33]
5	$e^- + Ar_m^* \rightarrow 2\ e^- + Ar^+$	Ionization of Ar_m^*	$\sigma(E)$	[34]
6	$e^- + Ar_m^* \rightarrow e^- + Ar^*$ (total)	Total excitation from Ar_m^*	$\sigma(E)$	[35]
7	$e^- + N_2\ (X) \rightarrow e^- + N_2\ (X)$	Elastic collision with N_2	$\sigma(E)$	[36]
8	$e^- + N_2\ (X) \rightarrow e^- + N_2\ (A)$	Electronic excitation of N_2	$\sigma(E)$	[36]
9	$e^- + N_2\ (X) \rightarrow e^- + N_2\ (B)$	Electronic excitation of N_2	$\sigma(E)$	[36]
9b	$e^- + N_2\ (X) \rightarrow e^- + N_2\ (B')$	Electronic excitation of N_2	$\sigma(E)$	[36][a]
10	$e^- + N_2\ (X) \rightarrow e^- + N_2\ (a')$	Electronic excitation of N_2	$\sigma(E)$	[36]
11	$e^- + N_2\ (X) \rightarrow e^- + N_2\ (a)$	Electronic excitation of N_2	$\sigma(E)$	[36]
12	$e^- + N_2\ (X) \rightarrow e^- + N_2\ (w)$	Electronic excitation of N_2	$\sigma(E)$	[36]
13	$e^- + N_2\ (X) \rightarrow e^- + N_2\ (C)$	Electronic excitation of N_2	$\sigma(E)$	[36]
14	$e^- + N_2\ (X) \rightarrow 2\ e^- + N_2^+$	Ionization of N_2	$\sigma(E)$	[36,37]
15	$e^- + N_2\ (X) \rightarrow 2\ e^- + N^+ + N$	Dissociative ionization of N_2	$\sigma(E)$	[38]
16	$e^- + N_2\ (X) \rightarrow e^- + 2\ N$	Dissociation of N_2	$\sigma(E)$	[36]
17	$e^- + N \rightarrow 2\ e^- + N^+$	Ionization of N	$\sigma(E)$	[39]
18	$e^- + e^- \rightarrow e^- + e^-$	Electron–electron Coulomb collisions	$\sigma(E)$	[40]
19	$e^- + Ar^+ + e^- \rightarrow Ar + e^-$	Three-body recombination with Ar^+	$k = 10^{-19}\ (T_e(K)/300)^{-4.5}\ cm^6\ s^{-1}$	[41]
20	$e^- + N^+ + e^- \rightarrow N + e^-$	Three-body recombination with N^+	$k = 5.4 \times 10^{-24}\ (T_e(eV))^{-4.5}\ cm^6\ s^{-1}$	[25]
21	$e^- + N^+ + Ar \rightarrow N + Ar$	Three-body recombination with N^+	$k = 6 \times 10^{-27}\ (300/T_e(K))^{1.5}\ cm^6\ s^{-1}$	[21]
22	$e^- + N^+ + N_2 \rightarrow N + N_2$	Three-body recombination with N^+	$k = 6 \times 10^{-27}\ (300/T_e(K))^{1.5}\ cm^6\ s^{-1}$	[21]
23	$e^- + N^+ + N \rightarrow N + N$	Three-body recombination with N^+	$k = 6 \times 10^{-27}\ (300/T_e(K))^{1.5}\ cm^6\ s^{-1}$	[21]
24	$e^- + N_2^+ \rightarrow N + N$	Dissociative recombination with N_2^+	$k = 4.8 \times 10^{-7}\ (300/T_e(K))^{0.5}\ cm^3\ s^{-1}$	[24]
25	$e^- + N_3^+ \rightarrow N_2 + N$	Dissociative recombination with N_3^+	$k = 2 \times 10^{-7}\ (300/T_e(K))^{0.5}\ cm^3\ s^{-1}$	[25]
26	$e^- + N_4^+ \rightarrow N_2 + N_2$	Dissociative recombination with N_4^+	$k = 2 \times 10^{-6}\ (300/T_e(K))^{0.5}\ cm^3\ s^{-1}$	[24]

[a] Note that reaction (9b) does not give rise to a new chemical species, but it is used also as production rate for the N_2 (B) level in the model, because the N_2 (B′) level is assumed to decay radiatively to the N_2 (B) level.

rigid sphere model for a mixture of two chemical species [65]. The mobilities of the ions were adopted from refs [66–68]. These continuity and transport equations for the various ions and the electrons are coupled to Poisson's equation, in order to obtain a self-consistent calculation of the electric field distribution.

Finally, boundary conditions of the continuity equations define what happens at the cell walls. The ions are assumed to be neutralized at the walls. All the excited species (of nitrogen molecules, as well as the Ar_m^* metastable atoms) are assumed to be depopulated at the walls, with 100% probability. Finally, the N (^{4}S) atoms are assumed to be partially "lost" at the walls, either due to adsorption ("sticking") or to recombination with formation of N_2 (X) molecules. Guerra has recently developed a dynamical Monte Carlo model to study the atomic nitrogen recombination on Si [69]. In [70] typical recombination coefficients are reported in the order of 0.5% for stainless steel at a N_2 pressure of 5 Torr, and about 0.75% at 1 Torr N_2 pressure. Other surface materials, such as boron nitride, silicon and aluminium, yield even lower values. These low values are explained by the fact that once N adsorbs on the surface, a protective molecular N_2 layer will be formed over the saturated atomic N layer, preventing the further adsorption of

Table 3
Overview of the chemical reactions taken into account in the model for the various positive ions, as well as the corresponding rate coefficients, and the references where these data were adopted from

No.	Reaction	Name	Rate constant	Ref
Ar^+ reactions				
27	$Ar^+ + N_2 \rightarrow Ar + N_2^+$	Charge transfer	$k = 4.45 \times 10^{-10}\ cm^3\ s^{-1}$	[27]
28	$Ar^+ + N \rightarrow Ar + N^+$	Charge transfer	$k = 4.45 \times 10^{-10}\ cm^3\ s^{-1}$	[a]
N^+ reactions				
29	$N^+ + N_2 \rightarrow N + N_2^+$	Charge transfer	$k = 4.45 \times 10^{-10}\ cm^3\ s^{-1}$	[a]
30	$N^+ + Ar \rightarrow N + Ar^+$	Charge transfer	$k = 6 \times 10^{-14}\ cm^3\ s^{-1}$	[a]
31	$N^+ + N + N \rightarrow N_2^+ + N$	Ion conversion	$k = 3.3 \times 10^{-31}\ (300/T_g(K))^{0.75}\ cm^6\ s^{-1}$	[21,25]
32	$N^+ + N + N_2 \rightarrow N_2^+ + N_2$	Ion conversion	$k = 10^{-29}\ cm^6\ s^{-1}$	[21,25]
33	$N^+ + N_2 + N_2 \rightarrow N_3^+ + N_2$	Ion conversion	$k = 9 \times 10^{-30}\ \exp(400/T_g(K))\ cm^6\ s^{-1}$	[21,25]
N_2^+ reactions				
34	$N_2^+ + N \rightarrow N_2 + N^+$	Charge transfer	$k = 2.4 \times 10^{-15} * T_g(K)\ cm^3\ s^{-1}$	[21,25]
35	$N_2^+ + Ar \rightarrow N_2 + Ar^+$	Charge transfer	$k = 2.81 \times 10^{-10}\ cm^3\ s^{-1}$	[27]
36	$N_2^+ + N_2 + N_2 \rightarrow N_4^+ + N_2$	Ion conversion	$k = 6.8 \times 10^{-29}\ (300/T_g(K))^{1.64}\ cm^6\ s^{-1}$	[44]
37	$N_2^+ + N + N_2 \rightarrow N_3^+ + N_2$	Ion conversion	$k = 9 \times 10^{-30}\ \exp(400/T_g(K))\ cm^6\ s^{-1}$	[21,25]
N_3^+ reactions				
38	$N_3^+ + N \rightarrow N_2^+ + N_2$	Ion conversion	$k = 6.6 \times 10^{-11}\ cm^3\ s^{-1}$	[21,25]
39	$N_3^+ + N_2 \rightarrow N_2 + N + N_2^+$	Ion conversion	$k = 6.6 \times 10^{-11}\ cm^3\ s^{-1}$	[a]
40	$N_3^+ + Ar \rightarrow N_2 + N + Ar^+$	Ion conversion	$k = 6.6 \times 10^{-11}\ cm^3\ s^{-1}$	[a]
N_4^+ reactions				
41	$N_4^+ + N_2 \rightarrow N_2^+ + N_2 + N_2$	Ion conversion	$k = 2.1 \times 10^{-16}\ \exp(T_g(K)/121)\ cm^3\ s^{-1}$	[24]
42	$N_4^+ + N \rightarrow N^+ + 2\ N_2$	Ion conversion	$k = 10^{-11}\ cm^3\ s^{-1}$	[21,25]
43	$N_4^+ + Ar \rightarrow Ar^+ + 2\ N_2$	Ion conversion	$k = 10^{-11}\ cm^3\ s^{-1}$	[a]

Note that the recombination reactions with electrons were already tabulated in Table 2, and are therefore not repeated here.
[a] Assumed in this work (see text).

Table 4
Overview of the chemical reactions taken into account in the model for the various neutral species, as well as the corresponding rate coefficients, and the references where these data were adopted from

No.	Reaction	Name	Rate coefficient	Ref.
N_2 (A) reactions				
44	N_2 (A)+N_2 (A)→N_2 (B)+N_2 (X)	Level conversion	$k=7.7\times10^{-11}$ cm^3 s^{-1}	[45]
45	N_2 (A)+N_2 (A)→N_2 (C)+N_2 (X)	Level conversion	$k=1.5\times10^{-10}$ cm^3 s^{-1}	[46]
46	N_2 (A)+N (^{4}S)→N_2 (X)+N (^{2}P)	Level conversion	$k=4\times10^{-11}$ cm^3 s^{-1}	[47]
47	N_2 (A)+N_2 (a′)→N_4^++e$^-$	Associative ionization	$k=9\times10^{-12}$ cm^3 s^{-1}	[24]
48	N_2 (A)+N_2 (a′)→N_2^++N_2 (X)+e$^-$	Ionization	$k=1\times10^{-12}$ cm^3 s^{-1}	[24]
N_2 (B) reactions				
49	N_2 (B)+N_2→N_2 (A)+N_2	Level conversion	$k=0.95\times3\times10^{-11}$ cm^3 s^{-1}	[23,48]
50	N_2 (B)+N_2→N_2 (X)+N_2	Level conversion	$k=0.05\times3\times10^{-11}$ cm^3 s^{-1}	[23,48]
51	N_2 (B)+Ar→N_2 (A)+Ar	Level conversion	$k=0.01\times3\times10^{-11}$ cm^3 s^{-1}	[24]
52	N_2 (B)→N_2 (A)+hν	Radiative decay	$A=2\times10^5$ s^{-1}	[49]
N_2 (a′) reactions				
53	N_2 (a′)+N_2→N_2 (B)+N_2	Level conversion	$k=1.9\times10^{-13}$ cm^3 s^{-1}	[50]
54	N_2 (a′)+Ar→N_2 (B)+Ar	Level conversion	$k=10^{-14}$ cm^3 s^{-1}	[24]
47	N_2 (A)+N_2 (a′)→N_4^++e$^-$	Associative ionization	$k=9\times10^{-12}$ cm^3 s^{-1}	[24]
48	N_2 (A)+N_2 (a′)→N_2^++N_2 (X)+e$^-$	Ionization	$k=1\times10^{-12}$ cm^3 s^{-1}	[24]
55	N_2 (a′)+N_2 (a′)→N_4^++e$^-$	Associative ionization	$k=0.9\times5\times10^{-11}$ cm^3 s^{-1}	[23,24]
56	N_2 (a′)+N_2 (a′)→N_2^++N_2 (X)+e$^-$	Ionization	$k=0.1\times5\times10^{-11}$ cm^3 s^{-1}	[23,24]
N_2 (a) reactions				
57	N_2 (a)+N_2→N_2 (a′)+N_2	Level conversion	$k=2.2\times10^{-11}$ cm^3 s^{-1}	[51]
58	N_2 (a)+Ar→N_2 (a′)+Ar	Level conversion	$k=1.3\times10^{-11}$ cm^3 s^{-1}	[51]
59	N_2 (a)→N_2 (X)+hν	Radiative decay	$A=1.7\times10^4$ s^{-1}	[51]
60	N_2 (a)→N_2 (a′)+hν	Radiative decay	$A=1.91\times10^4$ s^{-1}	[24]
N_2 (w) reactions				
61	N_2 (w)+N_2→N_2 (a)+N_2	Level conversion	$k=0.5\times2\times10^{-11}$ cm^3 s^{-1}	[24]
62	N_2 (w)+Ar→N_2 (a)+Ar	Level conversion	$k=0.5\times10^{-12}$ cm^3 s^{-1}	[24]
63	N_2 (w)→N_2 (a)+hν	Radiative decay	$A=6.4\times10^2$ s^{-1}	[52]
N_2 (C) reactions				
64	N_2 (C)→N_2 (B)+hν	Radiative decay	$A=2.74\times10^7$ s^{-1}	[24,53]
N (^{4}S) reactions				
65	N (^{4}S)+N (^{4}S)+N_2→N_2 (B)+N_2	Atomic recombination	$k_a=8.27\times10^{-34}\exp(500/T_g(K))$ cm^6 s^{-1}	[21,24]
66	N (^{4}S)+N (^{4}S)+Ar→N_2 (B)+Ar	Atomic recombination	$k=2/6.5\times k_a$	[24,54]
67	N (^{4}S)+N (^{4}S)+N_2→N_2 (a)+N_2	Atomic recombination	$k=0.05\times k_a$	[55]
68	N (^{4}S)+N (^{4}S)+Ar→N_2 (a)+Ar	Atomic recombination	$k=0.05\times k_a$	[55]
46	N_2 (A)+N (^{4}S)→N_2 (X)+N (^{2}P)	Level conversion	$k=4\times10^{-11}$ cm^3 s^{-1}	[47]
Ar_m* reactions				
5	Ar_m*+e$^-$→Ar$^+$+2 e$^-$	Electron impact ionization	σ(E)	[34]
6	Ar_m*+e$^-$→Ar*+e$^-$	Electron impact excitation	σ(E)	[35]
69	Ar_m*+e$^-$→Ar_r*+e$^-$	Electron quenching (= transfer to a nearby radiative level, which will decay to the ground state)	$k=2\times10^{-7}$ cm^3 s^{-1}	[56]
70	Ar_m*+Ar_m*→Ar^0+Ar$^+$+e$^-$	Metastable–metastable collisions	$k=6.4\times10^{-10}$ cm^3 s^{-1}	[57,58]
71	Ar_m*+Cu^0→Ar^0+Cu$^+$+e$^-$	Penning ionization of Cu	$k=2.6\times10^{-10}$ cm^3 s^{-1}	[59,60]
72	Ar_m*+Ar^0→Ar^0+Ar^0	Two-body collisions	$k=2.3\times10^{-15}$ cm^3 s^{-1}	[61]
73	Ar_m*+2 Ar^0→Ar_2*+Ar^0	Three-body collisions	$k=1.4\times10^{-32}$ cm^6 s^{-1}	[61]
74	Ar_m*+N_2→Ar^0+N+N	Quenching by dissociation of N_2	$k=3.6\times10^{-11}$ cm^3 s^{-1}	[62–64]

The reactions of N_2(X) are not separately listed in the table, as they occur with all other reactive species, and are therefore listed already in this table and in previous Tables 2 and 3. Note that reactions 46, 47 and 48 are presented twice in the table, as they occur between two different kinds of reactive species. Reactions 5 and 6 were also listed in Table 2, and the cross sections as a function of energy are depicted in Fig. 2.

N atoms on the surface [70]. This explanation clarifies also why the recombination decreases for higher N_2 pressures. However, it was suggested that small impurities of O_2 might be responsible for an increase in the recombination rate, due to the wall recombination into NO molecules [70]. It should be noted that in our conditions, the N_2 pressure is typically lower, as the N_2 is only present as an impurity in the gas mixture, so that the formation of a protective N_2 layer will be less probable. In the context of TiN_x thin film deposition, Mao et al. [71,72] have reported sticking coefficients of N atoms on TiN_x layers varying from 0.1 for Ti-rich films to 0.003 for N-rich layers. In our case, the cell walls are metallic, so that a sticking coefficient of 0.1 is more probable. However, the value can also be lower, due to this protective N_2 layer formation, as mentioned above. Also, other cell walls, such as Cu, might give rise to a lower sticking coefficient of N [73]. Therefore, in our calculations, we have assumed a value of 0.05 for the sticking (adsorption) coefficient of N (^{4}S) atoms. Furthermore, when the N atoms adsorb, we assume at the same time that they will recombine with adsorbed N atoms (i.e., assuming that the walls are saturated with N), resulting in the formation of N_2 molecules. However, we have also run calculations, varying this value of the sticking coefficient in the range 0.005–1, to investigate the effect of this assumed value (see below).

3. Results and discussion

Calculations are performed for a Grimm-type glow discharge cell, with simplified cylindrical geometry of 4 mm diameter and 1 cm length, because it was demonstrated [74] that the plasma is mainly confined in this region close to the cathode. The discharge voltage is assumed to be 800 V, the pressure is 850 Pa and the electrical current is about 15 mA. The N_2 gas concentration is varied between 0.1 and 10% (v/v) of the total gas mixture.

3.1. Electrons and various positive ions

3.1.1. Calculated number densities

Fig. 3 illustrates the calculated two-dimensional density profiles of the electrons and the various positive ions, for a N_2 concentration of 1%. The cathode is found at the left side of the figures, whereas the other borders of the figures represent the cell walls at anode potential.

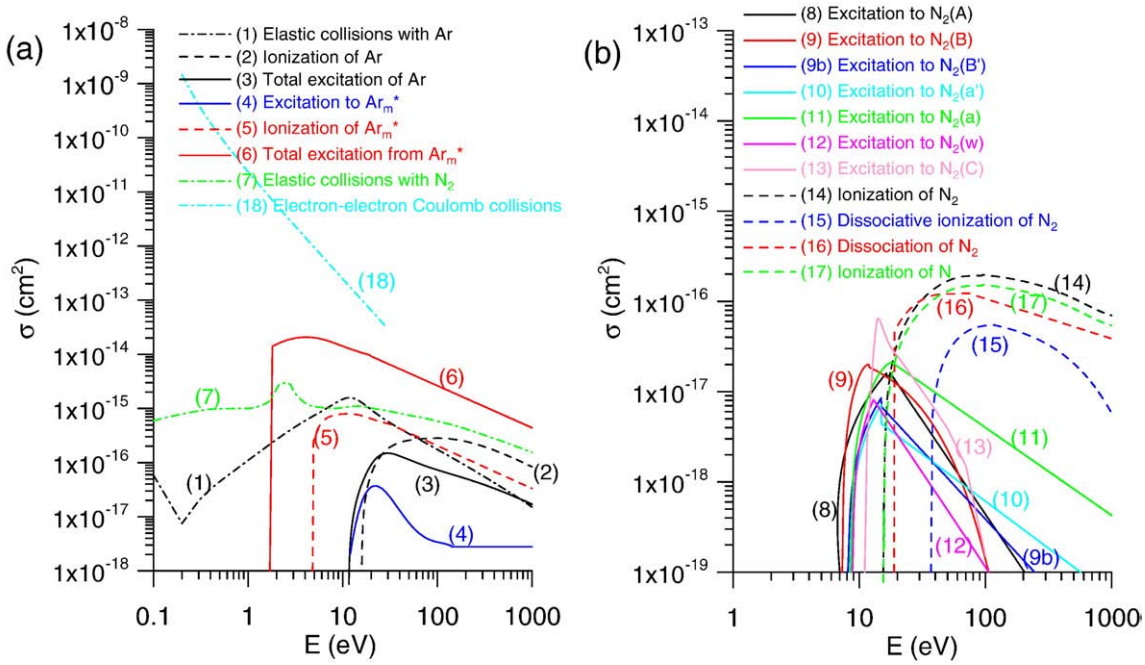

Fig. 2. Cross sections of the electron-impact collisions as a function of electron energy. (a) Collisions with Ar atoms (in ground state and metastable level), as well as the elastic collisions with N_2 molecules and the electron–electron Coulomb collisions. (b) Collisions with the N_2 molecules and N atoms. The solid lines represent electron-impact excitation collisions, the dashed lines are ionization and/or dissociation collisions, and the elastic collisions and the electron–electron Coulomb collisions are plotted with dash-dotted lines.

As is clear from this figure, the first cm from the cathode is indeed the most intense plasma region.

It is evident that at this low N_2 impurity, the Ar^+ ions (Fig. 3(b)) are the dominant ions, with a density more or less equal to the electron density (Fig. 3(a)). Indeed, the most important production mechanism for both the electrons and the Ar^+ ions is electron impact ionization of the Ar gas, as will be shown below.

The most important nitrogen-related ions are the N_2^+ ions, but as appears from Fig. 3(d), their density is about 2 orders of magnitude lower than the Ar^+ ion density, which reflects the gas ratio (1% N_2 vs.

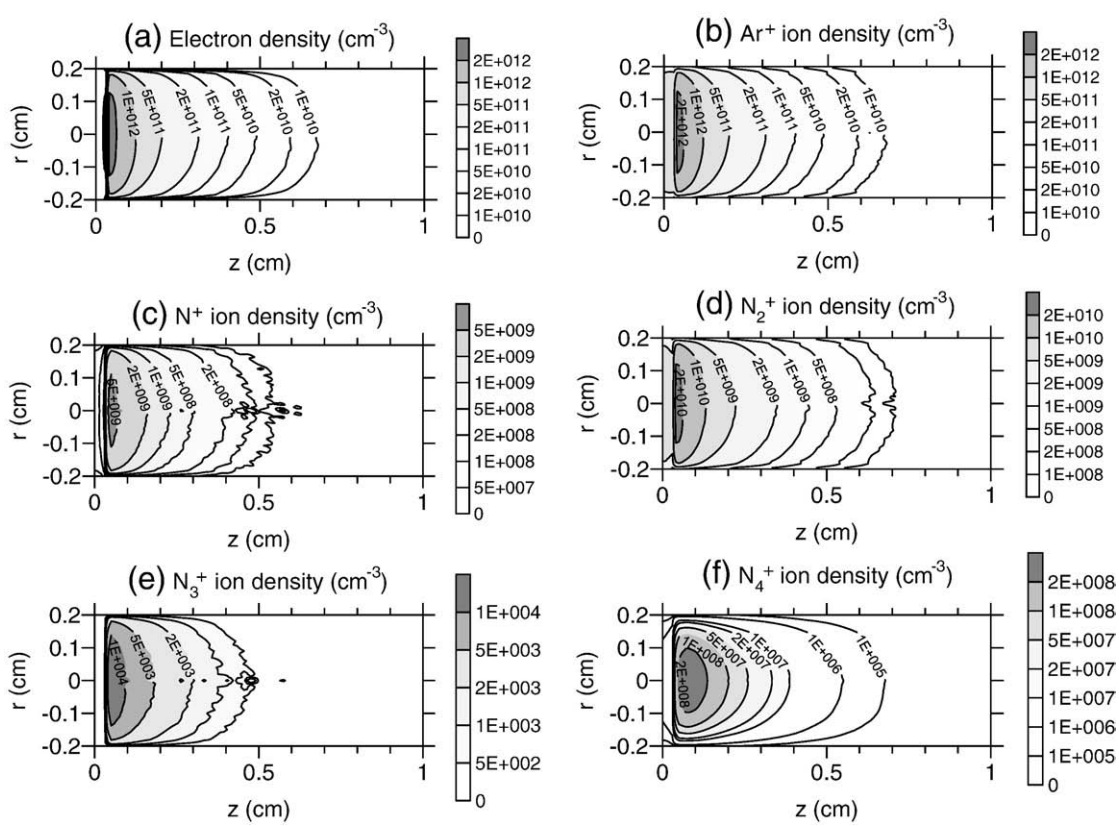

Fig. 3. Calculated two-dimensional density profiles of the electrons (a), Ar^+ (b), N^+ (c), N_2^+ (d), N_3^+ (e) and N_4^+ ions (f), at 1% of N_2 (v/v) added to the Ar gas.

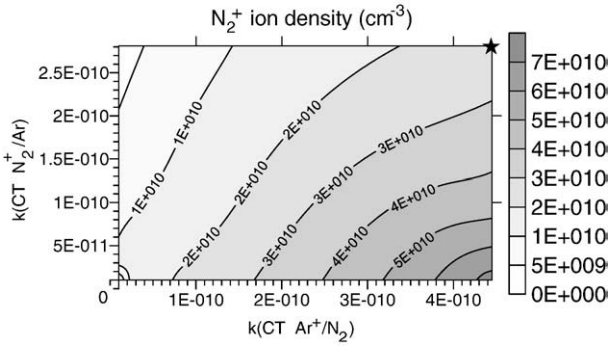

Fig. 4. Effect of the asymmetric charge transfer rate coefficients of N_2^+/Ar (i.e., reaction 35 of Table 3) and Ar^+/N_2 (i.e., reaction 27 of Table 3) on the calculated N_2^+ ion density at the maximum of its profile, for the same conditions as in Fig. 3. The symbol at the upper right corner of the figure corresponds to the combination of rate coefficients used as basic set of our calculations.

99% Ar). The N^+ ions (Fig. 3(c)) are a further factor of 4 lower, because they are mainly indirectly formed from the N_2 gas (i.e., first dissociation of N_2, followed by electron impact ionization of N atoms, or charge transfer between Ar^+ and N; see below). Nevertheless, they are more important than the N_4^+ and especially the N_3^+ ions, which are about two and six orders of magnitude lower in density than the N_2^+ ion density; see Fig. 3(e,f). The reason is that they are also only formed by two-step processes (see below), but they get lost more efficiently by dissociative recombination or ion conversion to Ar^+ (see Table 3). This result is different from atmospheric pressure glow discharges, where it was predicted that the N_4^+ ions can become the dominant nitrogen-related ions, even at impurities as low as 17 ppm N_2 [75]. On the other hand, in atmospheric pressure capillary surface wave discharges in He/N_2 mixtures, the N^+ ions were calculated to be the dominant ionic species, followed by N_2^+, N_3^+ and N_4^+ [25].

As mentioned above, we have made some assumptions for the rate coefficients of asymmetric charge transfer between Ar^+ ions and N_2 molecules, and between N_2^+ ions and Ar atoms, because it was reported in [42,43] that these rate coefficients can vary significantly, depending on the vibrational energy levels of N_2 or N_2^+. We have adopted the values used in [27], i.e., $k=4.45\times10^{-10}$ cm^3 s^{-1} for the reaction between Ar^+ and N_2, and $k=2.81\times10^{-10}$ cm^3 s^{-1} for the system N_2^+/Ar, because these calculations were validated by experiments [28]. However, these values are in the upper range of the values reported in [42,43]. Therefore, and also to investigate the sensitivity of the calculation results on these assumptions, we have also performed a set of calculations, varying the asymmetric charge transfer rate coefficients of both reactions in a somewhat lower range, as reported in refs [42,43], more specifically, $k=10^{-11}$–4.45×10^{-10} cm^3 s^{-1} for the reaction Ar^+/N_2 [42] and $k=10^{-11}$–2.81×10^{-10} cm^3 s^{-1} for the reaction N_2^+/Ar [43]. The effect on the calculated N_2^+ ion density, at the maximum of its profile, is plotted in Fig. 4. Note that the upper right corner of this figure represents the combination of rate coefficients used as basic set of our calculations. As expected, using lower values for the Ar^+/N_2 reaction yields lower values for the N_2^+ ion density, and lower values for the N_2^+/Ar reaction give rise to higher values for the N_2^+ ion density. However, the variation in resulting N_2^+ ion densities is not as large as the variation in the assumed rate coefficients, i.e., varying the rate coefficients over one order of magnitude results in a variation in N_2^+ ion densities of a factor of 3–4, as can be observed in Fig. 4. Nevertheless, it is clear that in the extreme situation of a high rate coefficient for Ar^+/N_2 and a low rate coefficient for N_2^+/Ar the resulting N_2^+ ion density is significantly higher than in the opposite case. On the other hand, if both rate coefficients are assumed to be lower (or higher) than the values adopted in our model, the N_2^+ ion density remains more or less unchanged. Finally, we have also checked the effect of these rate coefficients on the other calculation results. It is evident that varying the rate coefficients affects the relative importance of the various production and loss processes of the ions, but the effect on the resulting densities of electrons, Ar^+ ions and other nitrogen-related ions was found to be negligible. Therefore, the remaining of our calculations were performed with this basic set of rate coefficients, keeping in mind the uncertainty range for the N_2^+ ion density, as visualized in Fig. 4.

3.1.2. Effect of N_2 concentration on the densities

In Fig. 5, the electron and the various ion densities, at the maximum of their profiles, are plotted against N_2 concentration. It appears that the calculated electron and Ar^+ ion densities are nearly independent of the N_2 concentration, whereas all nitrogen-related ions clearly increase upon N_2 addition, as expected. The N_3^+ and N_4^+ ions increase more significantly, but the order of importance ($N_2^+>N^+>N_4^+>N_3^+$) remains unchanged for all Ar/N_2 gas mixtures investigated. At 10% N_2 addition, the maximum N_2^+ ion density is about twice the maximum N^+ ion density (i.e., about 6×10^{11} vs. 3×10^{11} cm^{-3}), and both densities are roughly one order of magnitude lower than the maximum Ar^+ density (i.e., 4.8×10^{12} cm^{-3}), which corresponds with the 10/90 gas ratio. The fact that the Ar^+ density is not decreasing upon N_2 addition is a bit surprising, because it reacts away by asymmetric charge transfer with N_2 and N, with formation of N_2^+ and N^+ ions (see below), but on the other hand, it is also created from asymmetric charge transfer of N_2^+ ions with the Ar gas, and both processes seem to cancel out each other. However, as mentioned above, the rate coefficients of these charge transfer processes are subject to large uncertainties, and the results might look different when other rate coefficients will be used. Comparison with experimental data, when they become available for these conditions of analytical glow discharges, can hopefully bring more clarification on the importance of both charge transfer processes.

3.1.3. Calculated contributions of various production and loss mechanisms

The effect of the N_2 concentration in the Ar/N_2 gas mixture on the relative contributions of the various production and loss processes for the electrons and the various ions is illustrated in Fig. 6. As mentioned above, electron impact ionization of the Ar gas is the dominant production mechanism for both the electrons and the Ar^+ ions, certainly for low N_2 gas concentrations (see Fig. 6(a) and (b)). Electron impact ionization and dissociative ionization of the N_2 gas are only of minor importance for the electron production, at all N_2 additions under study. At 10% N_2 concentration, electron impact ionization of N_2 contributes for about 6%, whereas dissociative ionization remains negligible, with a maximum contribution of about 1%. For the production of Ar^+ ions, it appears from Fig. 6(b) that charge transfer from N_2^+ ions becomes more important than electron impact ionization of Ar, at 10% N_2 addition, with

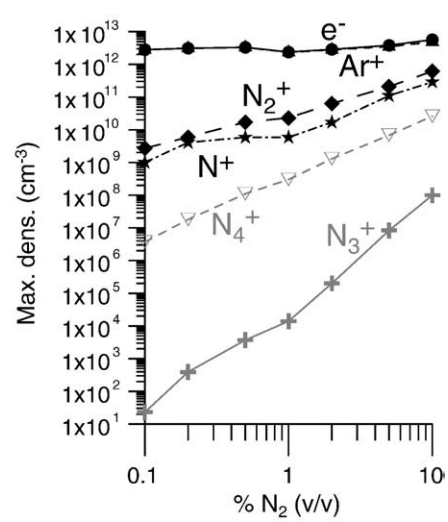

Fig. 5. Calculated densities of electrons, Ar^+, N^+, N_2^+, N_3^+ and N_4^+ ions, at the maximum of their profiles, for different percentages (v/v) of N_2 concentration.

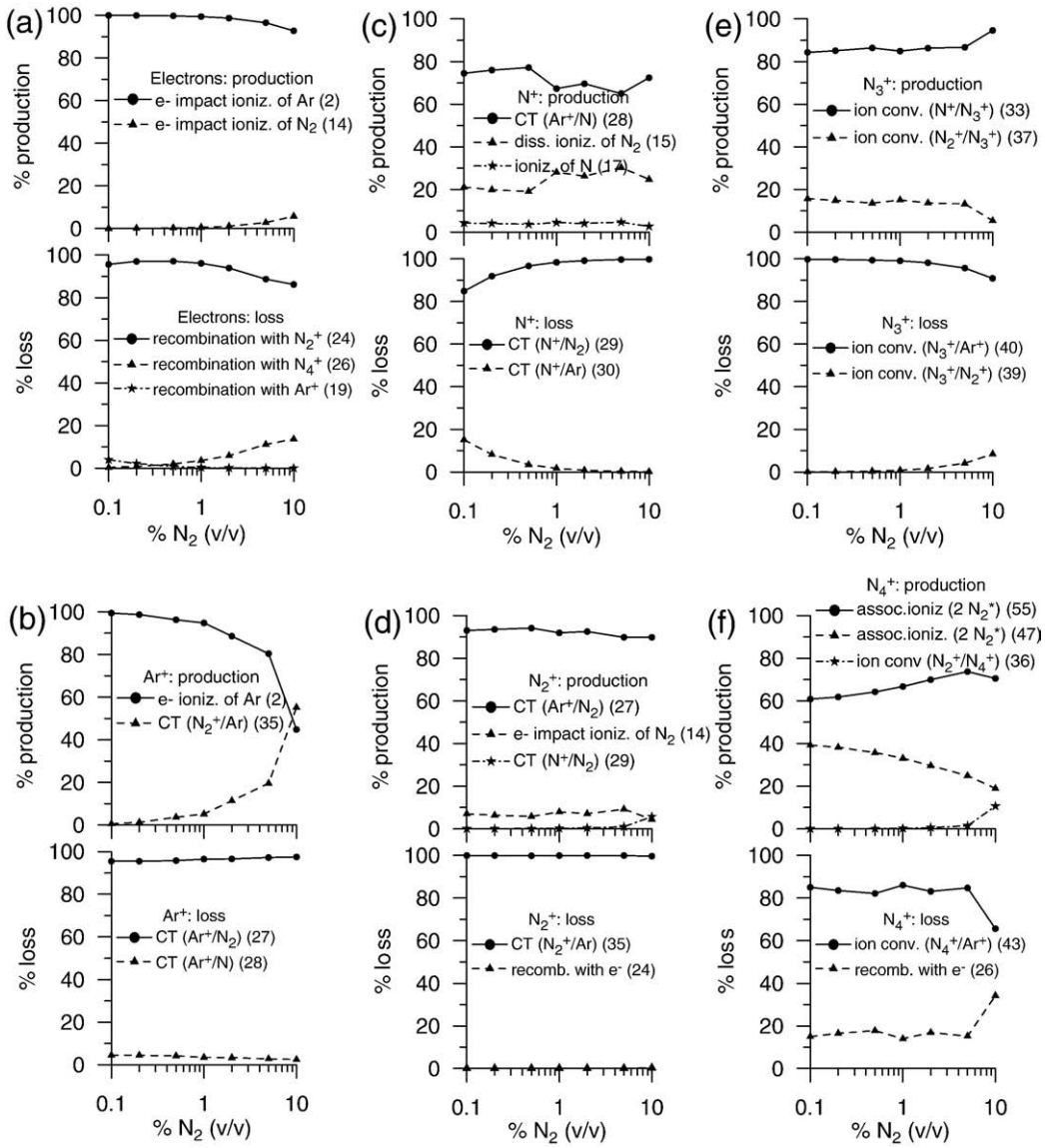

Fig. 6. Calculated relative contributions of the most important production and loss processes for the electrons (a), Ar^+ (b), N^+ (c), N_2^+ (d), N_3^+ (e) and N_4^+ (f) ions, integrated over the entire discharge region, for different percentages (v/v) of N_2 concentration. The numbers between brackets after the production and loss processes correspond to the numbers given in Tables 2–4, to visualize the reaction processes.

the assumed rate coefficient of $k = 2.81 \times 10^{-10}$ cm^3 s^{-1}, but as mentioned above, this rate coefficient is subject to large uncertainties, which is hence reflected also in the relative importance of this process. As far as the loss of electrons and Ar^+ ions is concerned, recombination with N_2^+ ions is most important as loss mechanism for the electrons, as is clear from Fig. 6(a). Recombination with N_4^+ is of minor importance, due to its lower density, with a maximum contribution of around 10% at the highest N_2 concentration investigated. Recombination with N_3^+ ions is entirely negligible, and recombination with Ar^+ ions comes only into play at the lowest N_2 concentration investigated, because of the lower rate coefficient of this process, compared to dissociative recombination (see Table 2 above). For the Ar^+ ions, Fig. 6(b) illustrates that they are mainly lost by charge transfer with N_2, giving rise to N_2^+ ions, whereas charge transfer with N atoms, giving rise to N^+ ions contributes for less than 5%, at all Ar/N_2 gas mixtures investigated.

These two processes are the dominant production mechanisms for both the N^+ and N_2^+ ions, as can be deduced from Fig. 6(c) and (d), respectively. Besides this, electron impact dissociative ionization of N_2 contributes for about 20–30% to the production of N^+ ions, whereas the contribution of electron impact ionization of N atoms is as low as 3–5% (see Fig. 6(c)). Similarly, for the N_2^+ ions, electron impact ionization of N_2 contributes for at maximum 9% (see Fig. 6(d)). As observed in Fig. 6(c), the N^+ ions are mainly lost by charge transfer with N_2, giving rise to N_2^+ ions, but at very low N_2 concentrations, charge transfer with Ar atoms can contribute for about 15% (at 0.01% N_2 addition). On the other hand, charge transfer with Ar atoms is calculated to be the dominant loss mechanism for the N_2^+ ions, as is clear from Fig. 6(d).

The N_3^+ ions (Fig. 6(e)) are mainly created by conversion from N^+ ions, in a three-body process with two N_2 molecules (i.e., reaction 33 of Table 2), explaining the pronounced increase of N_3^+ ion density upon N_2 addition, see Fig. 5 above. They are predominantly destroyed by conversion into Ar^+ ions, upon collision with Ar atoms (i.e., reaction 40 of Table 3). Finally, Fig. 6(f) illustrates that the most important production process for the N_4^+ ions is associative ionization by collision of two N_2 molecules in excited levels (reactions 47 and 55 of Table 4), whereas conversion into Ar^+ ions, as well as (to a lower extent) dissociative recombination with electrons, are the dominant loss mechanisms (see Fig. 6(f)).

3.2. Neutral species

3.2.1. Calculated number densities of N_2 molecules and N atoms, and dissociation degree

The two-dimensional density profiles of the N_2 molecules and N atoms, for 1% N_2 addition, are illustrated in Fig. 7. As appears from Fig. 7(a), the N_2 molecule density is in the order of 2×10^{15} cm^{-3} in the largest part of the Grimm-type cell (note that in reality, the latter extends after 1 cm from the cathode, as mentioned above). This value corresponds indeed to about 1% of the Ar gas density. However, it drops to values of 1.3×10^{15} cm^{-3} near the cathode, where dissociation takes place. The latter process gives rise to the formation of the N atoms, which correspondingly exhibit a maximum density near the cathode (see Fig. 7(b)).

By comparing the N atom and N_2 molecule densities, integrated over the entire simulated discharge region, a value for the dissociation degree was estimated to be 1.4%, for a N_2 concentration of 1%. For analytical Grimm-type conditions, the dissociation degree of N_2 has not yet been determined to the author's knowledge, and only indirect information can be obtained from optical emission spectra and mass spectral intensities, but these data are also affected by end-on observation, Einstein transition probabilities, etc for GD-OES, and transfer of ions through the interface, possibly with a secondary discharge, etc for GDMS [73]. Other modeling studies, based on a similar set of reactions as in our model, reported N_2 dissociation degrees in the order of 0.1 to a few % for the positive column of a pure N_2 low pressure glow discharge [23], and about 10–20% for an atmospheric pressure capillary surface wave discharge in a He/N_2 mixture at 1% N_2 concentration [25]. This illustrates that the dissociation degree can vary dramatically depending on the kind of discharge and the operating conditions. On the other hand, the calculated dissociation degree of N_2 is in the same order of magnitude as the dissociation degree of H_2, calculated for similar (Grimm-type) conditions [76], although the important plasma species and their corresponding reactions are found to be quite different in both gas mixtures.

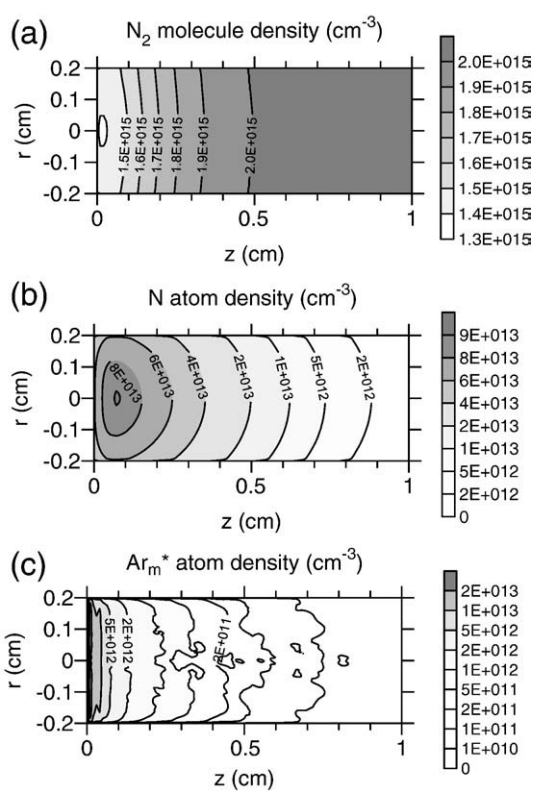

Fig. 7. Calculated two-dimensional density profiles of the N_2 molecules (a), N atoms (b) and Ar_m* metastable atoms (c), at 1% of N_2 (v/v) added to the Ar gas.

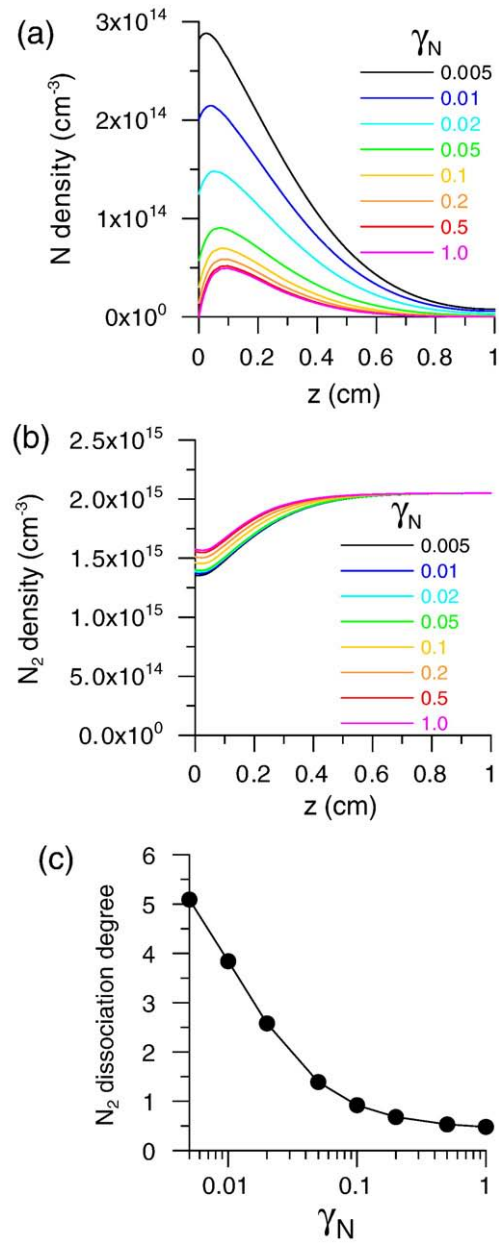

Fig. 8. Effect of the assumed sticking coefficient of the N atoms on the calculated one-dimensional density profiles of the N atoms (a) and N_2 molecules (b), and on the N_2 dissociation degree, at 1% of N_2 (v/v) added to the Ar gas.

3.2.2. Effect of N sticking coefficient on the densities

Another parameter, affecting the N atom (and N_2 molecule) density, and hence the dissociation degree, is the sticking coefficient of N atoms at the cell walls. As mentioned above, the N atoms arriving at the walls can either be reflected, or they can adsorb on the walls or recombine with adsorbed N atoms, with the formation of N_2 molecules. The latter two processes represent a loss of N atoms. Recombination coefficients were reported in the literature in the order of 0.5–0.75% for stainless steel, at N_2 pressures in the range 1–5 Torr, increasing for lower N_2 pressures [70]. On the other hand, sticking coefficients of N atoms on TiN_x layers were reported from 0.1 for Ti-rich films to 0.003 for N-rich films [71,72]. In our calculations, a value of 0.05 was assumed for the sticking (and recombination) coefficient of N atoms, but to investigate the effect of this assumed value on the

calculated N atom and N_2 densities and on the N_2 dissociation degree, we have run additional calculations, where this parameter was varied in the range 0.005–1. The result, for an Ar/N_2 gas mixture of 1% N_2, is illustrated in Fig. 8.

As expected, the N atom density increases when using lower values for the sticking coefficient. The effect is, however, of minor importance for sticking coefficients in the range 0.1–1, but it becomes increasingly important for low values of the sticking coefficient (0.005–0.1). The same observation was also made several years ago for sputtered atoms in a glow discharge [77]. The effect of the sticking (and recombination) coefficient on the N_2 molecule density is of minor importance, which is logical because the majority of the N_2 molecules simply originate from the background gas itself. Combining the N atom and N_2 molecule densities gives us the dissociation degree, depicted in Fig. 8 (c). For an assumed sticking coefficient of 0.05, the dissociation degree was calculated to be 1.4%, and these values drop only slightly for sticking coefficients up to 1. However, for sticking coefficients below 0.05, the dissociation degree increases more significantly, up to a value of 5% for an assumed sticking coefficient of 0.005. This illustrates the typical uncertainty in the calculation results, depending on the assumed sticking coefficients.

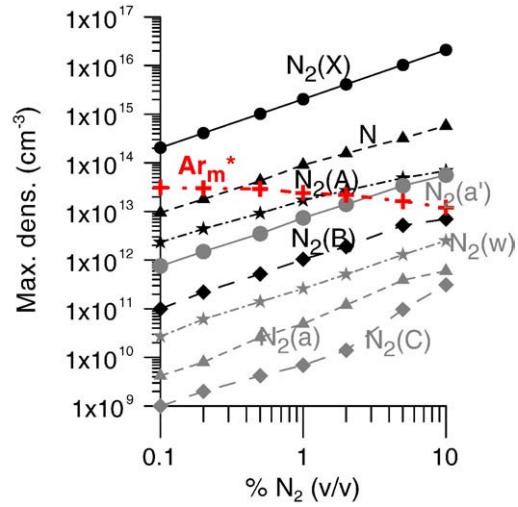

Fig. 10. Calculated densities of the N_2 ground state molecules, N atoms, Ar_m* metastable atoms and the various N_2 excited levels, at the maximum of their profiles, for different percentages (v/v) of N_2 concentration.

3.2.3. Calculated number densities of Ar metastable atoms and N_2 molecules in electronically excited levels

In Fig. 7(c), the Ar_m* metastable atom density was also shown, for comparison. It reaches a pronounced maximum of about 2×10^{13} cm^{-3} in front of the cathode, due to fast Ar^+ ion and Ar atom impact excitation [74], but it has overall values in the order of 10^{11}–10^{12} cm^{-3} further away from the cathode. Hence, this is clearly lower than the N_2 and N ground state populations, but it is comparable to the N_2 excited level populations. Indeed, the two-dimensional density profiles of the latter species, again for 1% N_2 addition, are plotted in Fig. 9.

The N_2 excited level populations all exhibit a similar profile, with a maximum near the cathode, as a result of electron impact excitation (see below). The N_2 (A) level has the highest population density, which is only two orders of magnitude lower than the N_2 ground state, as is clear from Fig. 9(a). It is followed by N_2 (a′) (Fig. 9(c)), N_2 (B) (Fig. 9(b)), N_2 (w) (Fig. 9(e)), N_2 (a) (Fig. 9(d)) and finally N_2 (C) (which has a population density almost 6 orders of magnitude lower than the N_2 ground level, see Fig. 9(f)). This order does not correspond exactly to the excitation energies of these levels (cf. Fig. 1), so it must be

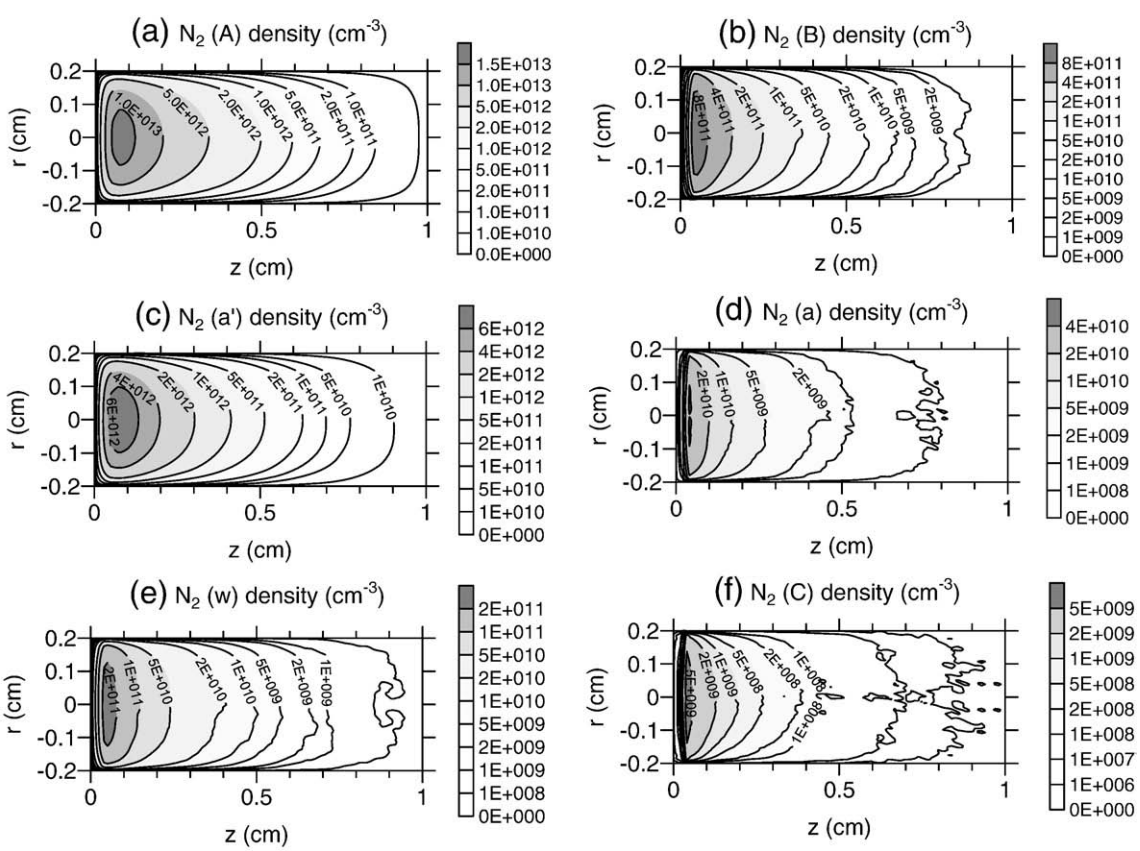

Fig. 9. Calculated two-dimensional density profiles of the various N_2 molecule excited levels, at 1% of N_2 (v/v) added to the Ar gas.

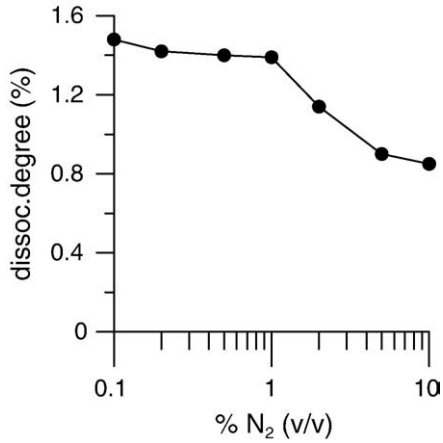

Fig. 11. Dissociation degree of N_2, calculated by integrating over the entire simulated discharge region, as a function of % N_2 (v/v) added to the Ar gas.

attributed to their production and loss processes, as will be explained below.

3.2.4. Effect of N_2 concentration on the densities and dissociation degree

Fig. 10 shows the effect of the N_2 concentration in the Ar/N_2 gas mixture on the densities of the N atoms, N_2 molecules in ground state and excited levels, and on the Ar_m* metastable levels, at the maximum of their profiles. It is clear that the densities of the N_2 molecules in the ground state and in most of the excited levels increase linearly with the N_2 addition. The N_2(C) excited state increases even a bit more than linearly, whereas the N_2(A) excited state increases slightly less than linearly. The fact that the N_2(C) excited state increases a bit more than linearly is in discrepancy with experimental data [5], showing that the emission intensity originating from the N_2(C) level did not increase linearly with the N_2 concentration. Because no self-absorption was detected in this second positive system, this suggests that the N_2(C) excited level should increase less than linearly upon N_2 addition. The reason for this discrepancy might be that an additional loss mechanism for the N_2(C) level, beside radiative decay to the N_2(B) level, needs to be included in the model, but we have found no information in the literature about the existence of another loss mechanism. Another explanation might be that the production of the N_2(C) level is overestimated at higher N_2 concentrations, but again, this is based on existing data (cross sections, rate coefficients) from literature. Alternatively, it might be that the vibrational kinetics affect the population of this level, and they are not yet taken into account in the model. It is planned to investigate this effect in the near future.

The N atom density increases a bit less than linearly upon N_2 addition, giving rise to a dissociation degree, which is slightly decreasing for higher N_2 additions, as can be observed in Fig. 11. Indeed, the dissociation degree of N_2 is in the order of 1.4–1.5% for Ar/N_2 gas mixtures up to 1% N_2, but for higher N_2 additions, it drops to a value of about 0.85% (for 10% N_2 addition).

The reason for this lower dissociation degree, and hence for the slightly less than linear increase of the N atom density upon N_2 addition in the gas mixture, can be found in the drop in Ar_m* metastable density, which is also illustrated in Fig. 10. Indeed, dissociation of N_2 upon collision with Ar_m* metastable atoms is the main production process for the N atoms, as will be shown below, but the Ar_m* metastable density drops upon N_2 addition, exactly as a result of this dissociation process, which results in quenching of the Ar_m* metastable atoms. A drop in the N_2 dissociation degree was also reported in [25], albeit for entirely different operating conditions, i.e., in atmospheric pressure capillary surface wave discharges in He/N_2 mixtures, where the dissociation degree was calculated to be 70% at very low N_2 concentrations (<0.05%) and decreases to about 10–20% at 1% N_2 addition. The same authors also reported a drop in He_m* metastable density upon N_2 addition [25]. Finally, for analytical Grimm-type glow discharges, it was reported that the self-reversal for the ArI 811.5 nm and ArI 763.5 nm resonance lines was reduced upon N_2 addition, which suggested a reduction in the Ar_m* metastable atom population [5]. This is indeed predicted by our model calculations, although the experimental drop seems to be more pronounced than the calculated drop.

3.2.5. Calculated contributions of various production and loss mechanisms

The relative contributions of the various production and loss processes for the N_2 molecules in the ground state, the N atoms and the Ar_m* metastable atoms are illustrated in Fig. 12 for different Ar/N_2 gas mixtures. The most important production process for the N_2 ground state molecules (=N_2(X)) is asymmetric charge transfer between N_2^+ ions and Ar atoms, as is clear from Fig. 12(a). However, this result should not be overestimated, because most of the N_2

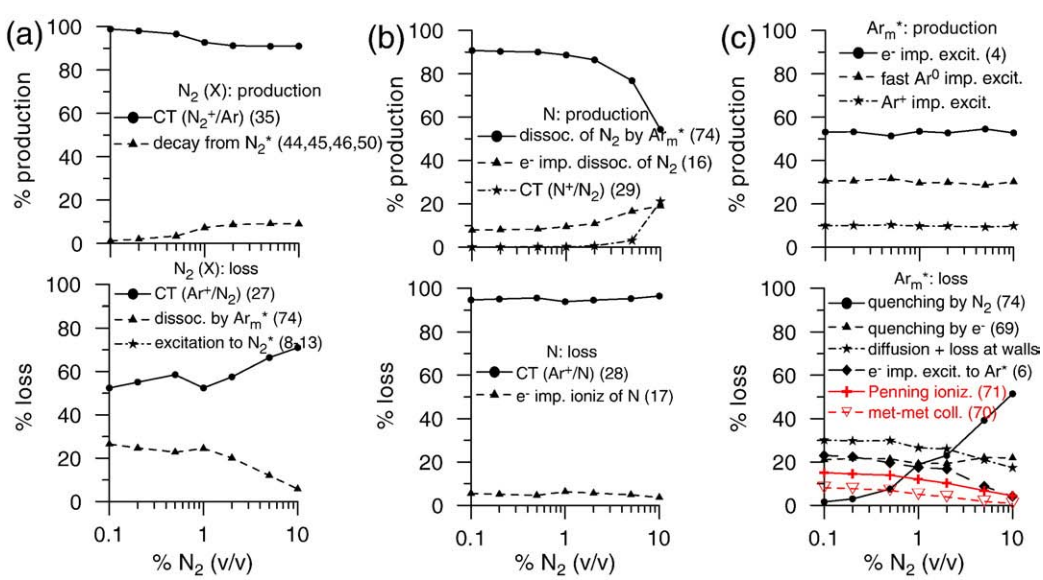

Fig. 12. Calculated relative contributions of the most important production and loss processes for the N_2 ground state molecules (a), N atoms (b), and Ar_m* metastable atoms (c), integrated over the entire discharge region, for different percentages (v/v) of N_2 concentration. The numbers between brackets after the production and loss processes correspond to the numbers given in Tables 2–4, to visualize the reaction processes.

ground state molecules simply enter the discharge as a result of the Ar/N_2 gas supply. The dominant loss mechanism for the N_2 ground state molecules is asymmetric charge transfer with Ar^+ ions, although dissociation upon collision with Ar_m* metastable atoms and electron impact excitation to higher N_2 levels also play a non-negligible role, as appears from Fig. 12(a).

As mentioned above, the N atoms are mainly created by dissociation of N_2 molecules upon collision with Ar_m* metastable atoms (see Fig. 12(b)), except at higher N_2 additions (because of the lower Ar_m* metastable atom density), where electron impact dissociation of N_2, as well as asymmetric charge transfer between N^+ and N_2 play a non-negligible role. As illustrated in Fig. 12(b), loss of the N atoms in the plasma is almost exclusively attributed to asymmetric charge transfer between Ar^+ ions and N atoms, although sticking at the walls, and/or recombination with adsorbed N atoms into N_2 molecules, can also not be neglected as loss mechanism for the N atoms.

The Ar_m* metastable atoms are mainly created by electron impact excitation, followed by fast Ar^0 impact excitation and fast Ar^+ impact excitation, and the relative importance of these production processes remains more or less the same for all Ar/N_2 gas mixtures investigated (see Fig. 12(c)). The latter does not hold true for the loss of the Ar_m* metastable atoms, where quenching upon collision with N_2 molecules (resulting in N_2 dissociation, see above) becomes increasingly important for higher N_2 concentrations, and is even the dominant loss mechanism above 2% N_2 addition. This trend is at the expense of the other loss mechanisms, such as diffusion and loss by de-excitation at the walls, quenching upon collision with electrons, electron impact excitation to higher Ar excited levels, Penning ionization of sputtered atoms and Ar_m* metastable–metastable collisions.

Finally, the relative contributions of the different production and loss processes for the N_2 molecules in the various excited levels are plotted against N_2 concentration in Fig. 13. In general, electron impact excitation from the $N_2(X)$ ground state molecules is a significant production process for most of the excited levels. For the $N_2(w)$ level (Fig. 13(e)), it is the only population mechanism taken into account in the model. For $N_2(B)$, $N_2(a)$ and $N_2(C)$, it is the most important production process, as can be seen from Fig. 13(b), (d) and (f), respectively, although other population mechanisms play a role as well. Indeed, for the $N_2(B)$ level (Fig. 13(b)),

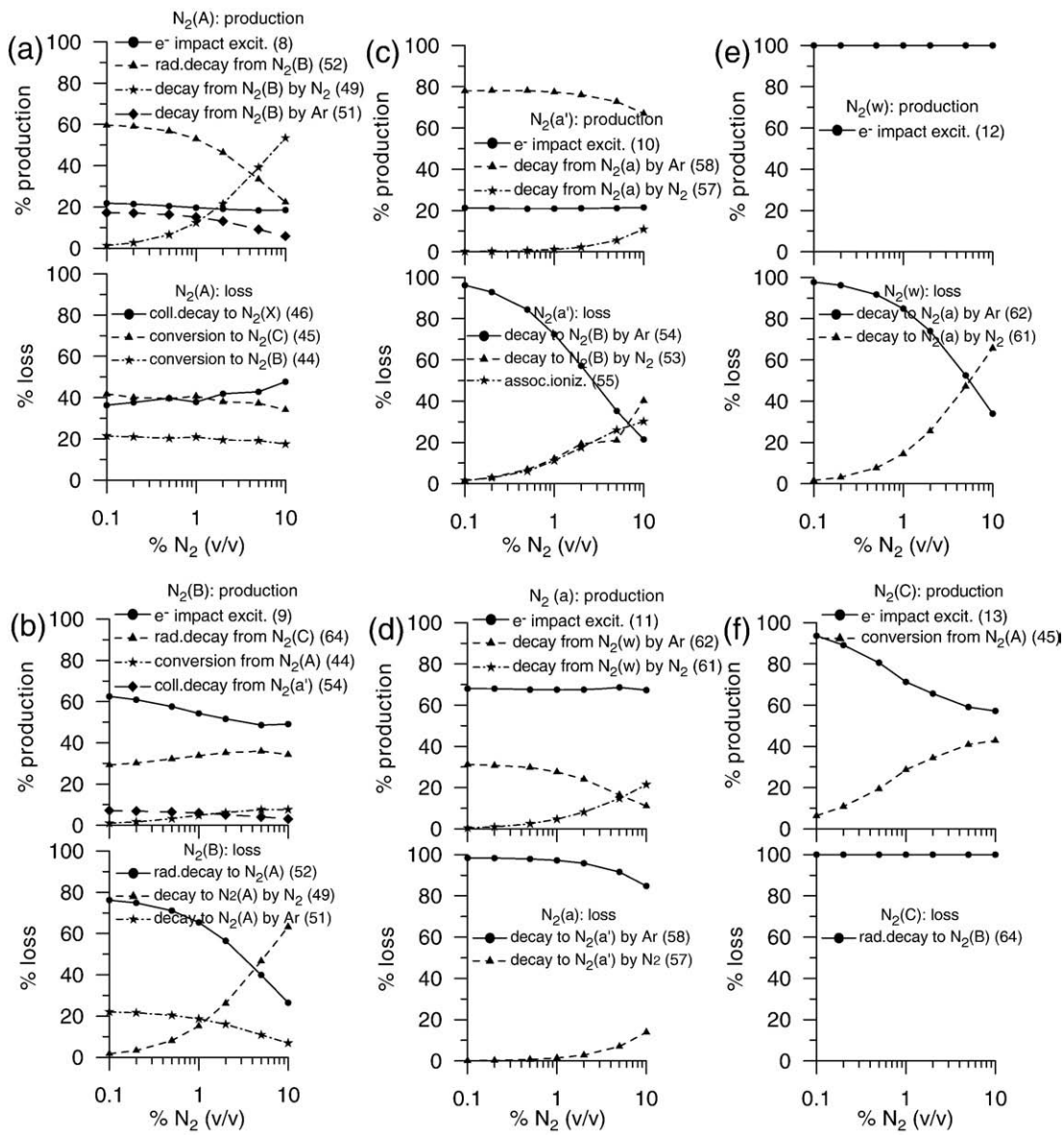

Fig. 13. Calculated relative contributions of the most important production and loss processes for the N_2 molecules in various excited levels, integrated over the entire discharge region, for different percentages (v/v) of N_2 concentration. (a) $N_2(A)$, (b) $N_2(B)$, (c) $N_2(a')$, (d) $N_2(a)$, (e) $N_2(w)$, (f) $N_2(C)$. The numbers between brackets after the production and loss processes correspond to the numbers given in Tables 2–4, to visualize the reaction processes.

radiative decay from the N_2(C) level contributes for about 30–35%. For the N_2(a) level (Fig. 13(d)), a similar contribution is observed for decay from the N_2(w) level upon collision with Ar atoms or N_2 molecules. Finally, the N_2(C) level (Fig. 13(f)) is also created by collision of two N_2 molecules in N_2(A) levels (i.e., conversion from N_2(A)), especially at higher N_2 additions. For the N_2(A) and N_2(a′) levels, electron impact excitation from the N_2(X) ground state contributes for only about 20% (see Fig. 13(a) and (c)), but these levels are predominantly populated by decay from higher excited levels. Indeed, N_2(A) is mainly formed by decay from N_2(B), either radiatively or upon collision with Ar atoms or N_2 molecules, as can be observed in Fig. 13(a). Similarly, decay from N_2(a) upon collision with Ar atoms is the dominant production process for the N_2(a′) level, as appears from Fig. 13(c).

As far as the loss of these levels is concerned, they are mainly depopulated either by (collisional or radiative) decay to lower levels, or by conversion into higher levels. N_2(A) decays for about 40% to the N_2(X) ground state upon collision with N atoms, and it is for about 40% converted into the N_2(C) level. The remaining 20% is converted into N_2(B), as is clear from Fig. 13(a). On the other hand, Fig. 13(b) illustrates that N_2(B) decays entirely to N_2(A), especially by emission of radiation, but also upon collisions with Ar or N_2 (the latter especially at higher N_2 additions). The next level, N_2(a′), decays mainly into N_2(B), upon collision with Ar or N_2, although associative ionization, with formation of N_4^+ ions, also comes into play, especially at higher N_2 additions (see Fig. 13(c)). Further, Fig. 13(d) and (e) shows that N_2(a) gets almost exclusively lost by decay into N_2(a′) upon collision with Ar atoms, whereas N_2(w) decays completely into N_2(a). Finally, N_2(C) decays radiatively into N_2(B).

Hence, the sequence of conversions and decays from and towards these excited N_2 levels can be summarized as follows: All levels are produced to some (larger or smaller) extent by electron impact excitation from the N_2(X) ground level. This is the only production process for the singlet N_2(w) level, which decays completely into the singlet N_2(a) level, by collision with Ar (or N_2), and N_2(a) decays further into the singlet N_2(a′) level, mainly upon collision with Ar. N_2(a′) then further decays into the triplet level N_2(B). The three triplet levels, i.e., N_2(A), N_2(B) and N_2(C), are also closely linked. Indeed, N_2(A) is mainly depopulated by decay to the ground level and by conversion into N_2(C), i.e., the highest level in our model. The latter completely decays into N_2(B) by emission of radiation, whereas N_2(B) decays entirely into N_2(A), especially radiatively, but also upon collision with Ar atoms or N_2 molecules. The close link between the N_2(A) and N_2(B) triplet states was also predicted by the model of Vasco and Loureiro [23]. Moreover, Bengtson demonstrated very strong emission from several bands of N_2, mostly from the $C\,^3\Pi_u$–$B\,^3\Pi_g$ system [2]. This corresponds well with our observations, because this radiative transition is indeed characterized by the highest Einstein transition probability (i.e., $A = 2.74 \times 10^7$ s^{-1}; see Table 4 above).

The latter explains also why the N_2(C) level has the lowest population density from all excited levels included in our model (see Fig. 9 above), because it is indeed very efficiently depopulated by radiative decay. As mentioned above, the population densities of the different excited levels do not correlate with their excitation energy, and this is attributed to their production and loss processes. The N_2(A) level has a high density, because it is created by several efficient processes, but it gets lost only upon collisions with other excited N_2 levels, which are of lower density than the N_2 ground state molecules or the Ar atoms. The N_2(B) level has a lower density than N_2(a′), because it gets lost efficiently by (radiative and collisional) decay into N_2(A), whereas the loss processes for the N_2(a′) level are characterized by small rate coefficients (see reactions 53 and 54 of Table 4), and moreover, it is created efficiently out of N_2(a) (i.e., reactions 57 and 58 of Table 4 are characterized by larger rate coefficients). The latter explains also why the N_2(a) level has a lower density than the N_2(w) level, which is again not so efficiently lost, due to rather small rate coefficients of the loss mechanisms. Hence, in this way, the population densities of the various excited levels can be explained by the relative importance of their production and loss processes.

4. Conclusion

We have developed a numerical model for a glow discharge in Ar/N_2 mixtures. 16 different plasma species are considered in the model, including Ar atoms in the ground state and the 4s metastable levels, N_2 molecules in the ground state and in six different electronically excited levels, N atoms, Ar^+, N^+, N_2^+, N_3^+ and N_4^+ ions, as well as electrons. 74 different chemical reactions are taken into account in the model, describing the production and loss of the different plasma species. Calculations were performed for a range of different Ar/N_2 gas mixtures, from 0.1 till 10% N_2 (v/v).

The two-dimensional number density profiles of all the plasma species are illustrated for 1% N_2 addition. The Ar^+ ions are the most important positive ions, followed by the N_2^+ ions (which are about two orders of magnitude lower in number density) and the N^+ ions (which are still a factor of 4 lower than the N_2^+ ion density). The densities of the other nitrogen-related ions, i.e., N_4^+ and N_3^+, are two and six orders of magnitude lower, respectively, than the N_2^+ ion density. They become, however, slightly more important at higher N_2 concentrations in the gas mixture, but the general order: $Ar^+ >> N_2^+ > N^+ >> N_4^+ >> N3^+$, remains the same for N_2 additions at least up to 10%.

Concerning the neutral species, the N_2 molecules in the ground state are the most important, beside the Ar gas atoms. The N_2 ground state density is fairly uniform throughout the discharge, except for a dip in front of the cathode, due to dissociation into N atoms. The latter have indeed a maximum density near the cathode, but integrated over the entire discharge region, their density is about two orders of magnitude lower than the N_2 density, giving rise to a dissociation degree of about 1.4% at 1% N_2 addition. However, it should be mentioned that the calculated N atom density depends quite strongly on the assumed sticking coefficient at the walls, especially for lower values of the sticking coefficient, as is also demonstrated in the paper. This also affects the dissociation degree, which varies from below 1% to above 5%, at 1% N_2 addition, for a sticking coefficient varying between 1 and 0.005. In general, the dissociation degree was calculated to be slightly higher for lower N_2 concentrations, but it drops more pronouncedly for higher N_2 additions, because the most significant dissociation mechanism, i.e., by collision with Ar_m* metastable atoms, becomes gradually less important. Indeed, the same process leads to quenching of the Ar_m* atoms, resulting in lower Ar_m* metastable densities for higher N_2 concentrations, which is in agreement with the literature.

The N_2 molecules in excited levels have clearly lower population densities than the N_2 ground state, by two orders of magnitude for the lowest excited level (i.e., N_2(A)) and by almost six orders for the highest level included in the model (i.e., N_2(C)). They are all characterized by a maximum near the cathode (attributed to electron impact excitation) and they all increase nearly to the same extent as the N_2 ground state, upon higher N_2 additions, so that the relative populations of excited levels remain more or less the same.

The relative contributions of the various production and loss mechanisms for the different plasma species were also calculated in the range of 0.1–10% N_2 addition. Electron impact ionization of Ar is the dominant production mechanism for the electrons and the Ar^+ ions, whereas the nitrogen-related ions are mainly produced by asymmetric charge transfer of Ar^+ ions (for N^+ and N_2^+), conversion from N^+ ions (for N_3^+) and associative ionization by two N_2 molecules in excited levels (for N_4^+). The electrons are almost exclusively lost by dissociative recombination with N_2^+ ions, whereas the ions are mainly lost by charge transfer or conversion into other ions. This is also the dominant loss mechanism for the N_2 ground state molecules and the N atoms. However, it should be mentioned that the rate coefficients for asymmetric charge transfer between Ar^+ and N_2, as well as the

opposite reaction, are subject to large uncertainties, and this can affect the calculation results, as is also illustrated in the paper.

Similarly, the N_2 molecules in excited levels appear also strongly linked by conversion into higher levels, upon collision with Ar atoms or N_2 molecules, and by (radiative or collisional) decay to lower levels. The sequence of conversions and decays can be summarized as follows: All levels are produced to some (larger or smaller) extent by electron impact excitation from the N_2(X) ground level. The lowest excited level, i.e., N_2 (A), is mainly depopulated by decay to the ground level and by conversion into N_2(C), i.e., the highest level in our model. The latter completely decays into N_2(B) by emission of radiation, whereas N_2(B) decays entirely into N_2(A). This close link between the N_2(B) and N_2(A) triplet states was also reported in literature. Furthermore, the other (singlet) levels are also closely linked. Indeed, N_2(w) decays completely into N_2(a); the latter decays further into N_2(a′), which in turn decays back into the triplet level N_2(B).

From these excited levels, some information can be obtained on optical emission intensities of N_2. However, it will also be of interest to investigate the effects of N_2 bands on analytical atomic emission lines. For this purpose, the vibrational distribution over the electronically excited N_2 molecules must be included in the model as well. This will also be necessary for a more detailed and accurate description of the Ar/N_2 glow discharge, because it is demonstrated that the vibrational and electron kinetics in N_2 containing discharges are strongly coupled (e.g., [14–20]). Indeed, superelastic collisions of electrons with vibrationally excited N_2 molecules will shift the electron energy distribution function towards higher energies, thus influencing the tail of this distribution. Therefore, the effect of the vibrational kinetics will be the subject of future work.

Acknowledgments

This research is financially supported by the European Marie Curie Research Training Network GLADNET (Contract No. MRTN-CT-2006 035459). The calculations were performed on the CALCUA supercomputer facilities of the University of Antwerp. Finally, we would like to thank V. Guerra and V. Hoffmann for the interesting discussions, as well as V. Guerra for supplying Fig. 1.

References

[1] A. Bengtson, Depth profiling of organic coatings with GDOES — investigation of molecular emission and interferences, J. Anal. At. Spectrom 18 (2003) 1066–1068.
[2] A. Bengtson, The impact of molecular emission in compositional depth profiling using glow discharge-optical emission spectrometry, Spectrochim. Acta Part B 63 (2008) 917–928.
[3] W. Fischer, A. Naoumidis, H. Nickel, Effects of a controlled addition of nitrogen and oxygen to argon on the analytical parameters of glow discharge optical emission spectrometry, J. Anal. At. Spectrom. 9 (1994) 375–380.
[4] K. Wagatsuma, Emission characteristics of mixed gas plasmas in low-pressure glow discharges, Spectrochim. Acta Part B 56 (2001) 465–486.
[5] P. Smid, E.B.M. Steers, Z. Weiss, J. Vlcek, The effect of nitrogen on analytical glow discharges studied by high resolution Fourier transform spectroscopy, J. Anal. At. Spectrom. 18 (2003) 549–556.
[6] B. Fernandez, N. Bordel, C. Perez, R. Pereiro, A. Sanz-Medel, The influence of hydrogen, nitrogen and oxygen additions to radiofrequency argon glow discharges for optical emission spectrometry, J. Anal. At. Spectrom. 17 (2002) 1549–1555.
[7] B. Fernandez, N. Bordel, R. Pereiro, A. Sanz-Medel, Investigations of the effect of hydrogen, nitrogen or oxygen on the in-depth profile analysis by radiofrequency argon glow discharge-optical emission spectrometry, J. Anal. At. Spectrom. 18 (2003) 151–156.
[8] L. Lobo, B. Fernandez, R. Pereiro, N. Bordel, A. Sanz-Medez, Nitrogen effects in multi-matrix calibrations by radiofrequency glow discharge-optical emission spectrometry, Anal. Bioanal. Chem. 389 (2007) 743–752.
[9] W.H. Long Jr., W.F. Bailey, A. Garscadden, Electron drift velocities in molecular-gas-rare-gas mixtures, Phys. Rev. A 13 (1976) 471–475.
[10] T. Kimura, K. Akatsuka, K. Ohe, Experimental and theoretical investigations of DC glow discharges in argon–nitrogen mixtures, J. Phys. D: Appl. Phys. 27 (1994) 1664–1671.
[11] E.B.M. Steers, P. Smid, V. Hoffmann, Z. Weiss, The effects of traces of molecular gases (H_2, N_2 & O_2) in glow discharges in noble gases, J. Phys.: Conf. Ser. 133 (2008) 012020.
[12] A. Ricard, A. Besner, J. Hubert, M. Moisan, High nitrogen atom yield downstream of an atmospheric pressure flowing Ar–N_2 microwave discharge, J. Phys. B, At. Mol. Opt. Phys. 21 (1988) L579–L583.
[13] D. Depla, S. Mahieu (Eds.), Reactive Sputter Deposition, Spring Series in Materials Science 109, Springer, Berlin, 2008.
[14] J. Loureiro, C.M. Fereira, Coupled electron energy and vibrational distribution functions in stationary N_2 discharges, J. Phys. D, Appl. Phys. 19 (1986) 17–35.
[15] C.M. Fereira, J. Loureiro, Electron excitation rates and transport parameters in high-frequency N_2 discharges, J. Phys. D, Appl. Phys. 22 (1989) 76–82.
[16] J. Loureiro, Time-dependent electron kinetics in N_2 and H_2 for a wide range of the field frequency including electron-vibration superelastic collisions, Phys. Rev. E 47 (1993) 1262–1275.
[17] J. Loureiro, A. Ricard, Electron and vibrational kinetics in an N_2–H_2 glow discharge with application to surface processes, J. Phys. D, Appl. Phys. 26 (1993) 163–176.
[18] M. Capitelli, M. Dilonardo, Non-equilibrium vibrational populations of diatomic species in electrical discharges: effects on the dissociation rates, Chem. Phys. 24 (1977) 417–427.
[19] V. Guerra, J. Loureiro, Non-equilibrium coupled kinetics in stationary N_2–O_2 discharges, J. Phys. D, Appl. Phys. 28 (1995) 1903–1918.
[20] V. Guerra, J. Loureiro, Self-consistent electron and heavy-particle kinetics in a low pressure N_2–O_2 glow discharge, Plasma Sources Sci. Technol. 6 (1997) 373–385.
[21] I.A. Kossyi, A. Yu Kostinsky, A.A. Matveyev van, V.P. Silakov, Kinetic scheme of the non-equilibrium discharge in nitrogen–oxygen mixtures, Plasma Sources Sci. Technol. 1 (1992) 207–220.
[22] C.M. Ferreira, B.F. Gordiets, E. Tatarova, Kinetic theory of low-temperature plasmas in molecular gases, Plasma Phys. Control. Fusion 42 (2000) B165–B188.
[23] V. Guerra, J. Loureiro, Electron and heavy particle kinetics in a low-pressure nitrogen glow discharge, Plasma Sources Sci. Technol. 6 (1997) 361–372.
[24] P.A. Sa, J. Loureiro, A time-dependent analysis of the nitrogen afterglow in N_2 and N_2–Ar microwave discharges, J. Phys. D, Appl. Phys. 30 (1997) 1320–2330.
[25] G.M. Petrov, J.P. Matte, I. Pérès, J. Margot, T. Sadi, J. Hubert, K.C. Tran, L.L. Alves, J. Loureiro, C.M. Ferreira, V. Guerra, G. Gousset, Numerical modelling of a He–N_2 capillary wave discharge at atmospheric pressure, Plasma Chem. Plasma Process 20 (2000) 183–207.
[26] E. Tatarova, F.M. Dias, C.M. Ferreira, A. Ricard, On the axial structure of a nitrogen surface wave sustained discharge: theory and experiment, J. Appl. Phys. 85 (1999) 49–62.
[27] J. Henriques, E. Tatarova, V. Guerra, C.M. Ferreira, Wave driven N_2–Ar discharge. I. Self-consistent theoretical model, J. Appl. Phys. 91 (2002) 5622–5631.
[28] J. Henriques, E. Tatarova, F.M. Dias, C.M. Ferreira, Wave driven N_2–Ar discharge. II. Experiment and comparison with theory, J. Appl. Phys. 91 (2002) 5632–5639.
[29] C.M. Ferreira, E. Tatarova, V. Guerra, B.F. Gordiets, J. Henriques, F.M. Dias, M. Pinheiro, Modeling of wave driven molecular (H_2, N_2, N_2–Ar) discharges as atomic sources, IEEE Trans. Plasma Sci. 31 (2003) 645–658.
[30] F. Debal, J. Bretagne, M. Jumet, M. Wautelet, J.P. Dauchot, M. Hecq, Analysis of DC magnetron discharges in Ar–N_2 gas mixtures. Comparison of a collisional-radiative model with optical emission spectroscopy, Plasma Sources Sci. Technol. 7 (1998) 219–229.
[31] A.B. Wedding, J. Borysow, A.V. Phelps, N_2 ($a''\,^1\Sigma_g^+$) metastable collisional destruction and rotational excitation transfer by N_2, J. Chem. Phys. 98 (1993) 6227–6234.
[32] A.V. Phelps, Z.L.j. Petrovic, Cold-cathode discharges and breakdown in argon: surface and gas phase production of secondary electrons, Plasma Sources Sci. Technol. 8 (1999) R21–R44.
[33] N.J. Mason, W.R. Newell, Total cross sections for metastable excitation in the rare gases, N. J. Mason and J. Phys. B 20 (1987) 1357–1377.
[34] H.A. Hyman, Electron-impact ionization cross sections for excited states of the rare gases (Ne, Ar, Kr, Xe), cadmium and mercury, Phys. Rev. A 20 (1979) 855–859.
[35] H.A. Hyman, Electron-impact excitation of metastable argon and krypton, Phys. Rev. A 18 (1978) 441–446.
[36] A. V. Phelps: ftp://jila.colorado.edu/collision_data.
[37] R.S. Freund, R.C. Wetzel, R.J. Shul, Measurements of electron-impact-ionization cross sections of N_2, CO, CO_2, CS, S_2, CS_2 and metastable N_2, Phys. Rev. A 41 (1990) 5861–5868.
[38] Y. Itikawa, M. Hayashi, A. Ichimura, K. Onda, K. Sakimoto, K. Takayanagi, M. Nakamura, H. Nishimura, T. Takayanagi, Cross sections for collisions of electrons and photons with nitrogen molecules, J. Phys. Chem. Ref. Data 15 (1986) 985–1010.
[39] A.C.H. Smith, E. Caplinger, R.H. Neynaber, E.W. Rothe, S.M. Trujillo, Electron impact ionization of atomic nitrogen, Phys. Rev. 127 (1962) 1647–1649.
[40] S. Hashiguchi, Numerical calculations for the electron energy distribution in a He hollow-cathode glow discharge, IEEE Trans. Plasma Sci. 19 (1991) 297–300.
[41] M.A. Biondi, in: E.W. McDaniel, W.L. Nighan (Eds.), Gas Lasers, Applied Atomic Collision Physics, Vol. 3, Academic Press, New York, 1982, Chapter 6.
[42] A.A. Viggiano, R.A. Morris, Rate constants for the reaction of Ar^+ ($^2P_{3/2}$) with N_2 as a function of N_2 vibrational temperature and energy level, J. Chem. Phys. 99 (1993) 3526–3530.
[43] S. Kato, J.A. de Gouw, C.D. Lin, V.M. Bierbaum, S.R. Leone, Charge-transfer rate constants for N_2^+ (v = 0–4) with Ar at thermal energies, Chem. Phys. Lett. 256 (1996) 305–311.
[44] H. Böhringer, F. Arnold, Temperature dependence of three-body association reactions from 45 to 400 K. The reactions $N_2^+ + 2\,N_2 \rightarrow N_4^+ + N_2$ and $O_2^+ + 2\,O_2 \rightarrow O_4^+ + O_2$, J. Chem. Phys. 77 (1982) 5534–5541.
[45] L.G. Piper, State-to-state N_2 ($A\,^3\Sigma_u^+$) energy pooling reactions. II. The formation and quenching of N_2 ($B\,^3\Pi_g$, v′ = 1–12), J. Chem. Phys. 88 (1988) 6911–6921.
[46] L.G. Piper, State-to-state N_2 ($A\,^3\Sigma_u^+$) energy pooling reactions. I. The formation of N_2 ($C\,^3\Pi_u$) and the Herman infrared system, J. Chem. Phys. 88 (1988) 231–239.
[47] L.G. Piper, The excitation of N (^2P) by N_2 ($A\,^3\Sigma_u^+$, v′ = 0,1), J. Chem. Phys. 90 (1989) 7087–7095.
[48] L.G. Piper, Energy transfer studies on N_2 ($X\,^1\Sigma_g^+$,v) and N_2 ($B\,^3\Pi_g$), J. Chem. Phys. 97 (1992) 270–275.

[49] L.G. Piper, The excitation of N_2 ($B\,^3\Pi_g$, v′ = 1–12) in the reaction between N_2 ($A\,^3\Sigma_u^+$) and N_2 (X, v ≥ 5), J. Chem. Phys. 91 (1989) 864–873.
[50] L.G. Piper, Quenching rate coefficients for N_2 ($a'\,^1\Sigma_u^-$), J. Chem. Phys. 87 (1987) 1625–1629.
[51] W.J. Marinelli, W.J. Kessler, B.D. Green, Quenching of N_2 ($a\,^1\Pi_g$, v′ = 0) by N_2, O_2, CO, CO_2, CH_4, H_2 and Ar, J. Chem. Phys. 90 (1989) 2167–2173.
[52] M.E. Fraser, W.T. Rawlins, Infrared (2 to 8 μm) fluorescence of the $W\,^3\Delta_u \rightarrow B\,^3\Pi_g$ and $w\,^1\Delta_u \rightarrow a\,^1\Pi_g$ systems of nitrogen, J. Chem. Phys. 88 (1988) 538–544.
[53] A. Lofthus, P.H. Krupenie, The spectrum of molecular nitrogen, J. Phys. Chem. Ref. Data 6 (1977) 113–307.
[54] A. Ricard, J. Tétreault, J. Hubert, Nitrogen atom recombination in high pressure Ar–N_2 flowing post-discharges, J. Phys. B: At. Mol. Opt. Phys. 24 (1991) 1115–1123.
[55] K.H. Becker, E.H. Fink, W. Groth, W. Jud, D. Kley, N_2 formation in the Lewis-Rayleigh afterglow, Faraday Discuss. Chem. Soc. 53 (1972) 35–51.
[56] C.M. Ferreira, A. Ricard, Modelling of the low-pressure argon positive column, J. Appl. Phys. 54 (1983) 2261–2271.
[57] C.M. Ferreira, J. Loureiro, A. Ricard, Populations in the metastable and the resonance levels of argon and stepwise ionization effects in a low-pressure argon positive column, J. Appl. Phys. 57 (1985) 82–90.
[58] L.A. Riseberg, W.F. Parks, L.D. Schearer, Penning ionization of Zn and Cd by noble-gas metastable atoms, Phys. Rev. A 8 (1973) 1962–1968.
[59] S. Inaba, T. Goto, S. Hattori, Determination of the Penning excitation cross sections of Mg atoms by He, Ne and Ar metastable atoms, J. Phys. Soc. Jpn 52 (1983) 1164–1167.
[60] K. Tachibana, Excitation of the $1s_5$, $1s_4$, $1s_3$ and $1s_2$ levels of argon by low-energy electrons, Phys. Rev. A 34 (1986) 1007–1015.
[61] A. Bogaerts, R. Gijbels, Two-dimensional model of a direct current glow discharge: description of the argon metastable atoms, sputtered atoms and ions, Anal. Chem. 68 (1996) 2676–2685.
[62] L.G. Piper, J.E. Velazco, D.W. Setser, Quenching cross sections for electronic energy transfer reactions between metastable argon atoms and noble gases and small molecules, J. Chem. Phys. 59 (1973) 3323–3340.
[63] M. Bourène, J. Le Calvé, De-excitation cross sections of metastable argon by various atoms and molecules, J. Chem. Phys. 58 (1973) 1452–1458.
[64] J.E. Velazco, J.H. Kolts, D.W. Setser, Rate constants and quenching mechanisms for the metastable states of Ar, Kr and Xe, J. Chem. Phys. 69 (1978) 4357–4373.
[65] J.O. Hirschfelder, C.F. Curtiss, R.B. Bird, Molecular Theory of Gases and Liquids, Wiley, New York, 1964.
[66] H.W. Ellis, R.Y. Pai, E.W. McDaniel, E.A. Mason, L.A. Viehland, Transport properties of gaseous ions over a wide energy range, At. Data Nucl. Data Tables 17 (1976) 177–210.
[67] H.W. Ellis, M.G. Thackston, E.W. McDaniel, E.A. Mason, Transport properties of gaseous ions over a wide energy range, Part III, At. Data Nucl. Data Tables 31 (1984) 113–151.
[68] L.A. Viehland, E.A. Mason, Transport properties of gaseous ions over a wide energy range, Part IV, At. Data Nucl. Data Tables 60 (1995) 37–95.
[69] V. Guerra, J. Loureiro, Dynamical Monte Carlo simulations of surface atomic recombination, Plasma Sources Sci. Technol. 13 (2004) 85–94.
[70] S.F. Adams, T.A. Miller, Surface and volume loss of atomic nitrogen in a parallel plate rf discharge reactor, Plasma Sources Sci. Technol. 9 (2000) 248–255.
[71] D. Mao, K. Tao, J. Hopwood, Ionized physical vapor deposition of titanium nitride: plasma and film characterization, J. Vac. Sci. Technol. A 20 (2002) 379–387.
[72] D. Mao, J. Hopwood, Ionized physical vapor deposition of titanium nitride: a deposition model, J. Appl. Phys. 96 (2004) 820–828.
[73] V. Hoffmann, private communication.
[74] A. Bogaerts, R. Gijbels, Comprehensive description of a Grimm-type glow discharge source used for optical emission spectrometry: a mathematical simulation, Spectrochim. Acta Part B 53 (1998) 437–462.
[75] T. Martens, A. Bogaerts, W.J.M. Brok, J. van Dijk, The dominant role of impurities in the composition of high pressure noble gas plasmas, Appl. Phys. Lett. 92 (2008) 041504.
[76] A. Bogaerts, Computer simulations of argon-hydrogen Grimm-type glow discharges, J. Anal. At. Spectrom. 23 (2008) 1476–1486.
[77] A. Bogaerts, J. Naylor, M. Hatcher, W.J. Jones, R. Mason, Influence of sticking coefficients on the behavior of sputtered atoms in an argon glow discharge: modeling and comparison with experiment, J. Vac. Sci. Technol. A 16 (1998) 2400.